

Field biotite weathering rate determination using U-series disequilibria

Sophie Rihs, Adrien Gontier, Alexandre Voinot, François Chabaux, Eric Pelt, Damien Lemarchand, Marie-Pierre Turpault

▶ **To cite this version:**

Sophie Rihs, Adrien Gontier, Alexandre Voinot, François Chabaux, Eric Pelt, et al.. Field biotite weathering rate determination using U-series disequilibria. Geochimica et Cosmochimica Acta, 2020, 276, pp.404 - 420. 10.1016/j.gca.2020.01.023 . hal-03490193

HAL Id: hal-03490193
https://hal.science/hal-03490193

Submitted on 20 May 2022

HAL is a multi-disciplinary open access archive for the deposit and dissemination of scientific research documents, whether they are published or not. The documents may come from teaching and research institutions in France or abroad, or from public or private research centers.

L'archive ouverte pluridisciplinaire **HAL**, est destinée au dépôt et à la diffusion de documents scientifiques de niveau recherche, publiés ou non, émanant des établissements d'enseignement et de recherche français ou étrangers, des laboratoires publics ou privés.



Distributed under a Creative Commons Attribution - NonCommercial 4.0 International License

Version of Record: https://www.sciencedirect.com/science/article/pii/S0016703720300351
Manuscript_e70053c38fab7beb5a31d7bc3b8baffa

Field biotite weathering rate determination using U-series disequilibria

RIHS Sophie[a*$], GONTIER Adrien[a*],
VOINOT Alexandre[a,§], CHABAUX François[a], PELT Eric[a], LEMARCHAND Damien[a], TURPAULT Marie-Pierre[b]

[a] Laboratoire d'Hydrologie et de Géochimie de Strasbourg, EOST, Université de Strasbourg and CNRS, 1 rue Blessig, 67084 Strasbourg cedex, France.

[b] Laboratoire de Biogéochimie des Ecosystèmes Forestiers, INRA, Champenoux, France

§ present address: Queen's Facility for Isotope Research, Department of Geological Sciences and Geological Engineering, Miller Hall, 36 Union St, K7L3N6 Kingston, Ontario, Canada

* Equal contribution from the first two authors.

[$] Corresponding author: rihs@unistra.fr

© 2020 published by Elsevier. This manuscript is made available under the CC BY NC user license
https://creativecommons.org/licenses/by-nc/4.0/

Abstract

The chemical weathering rate of silicates is a key parameter of several geochemical processes; however, the long-term field measurement of these rates remains challenging. Currently, there are several methods for quantifying field weathering rates, but each presents it's own unique set of difficulties. In this study uranium-series nuclides were used to investigate long-term biotite weathering in a soil profile. For this purpose, pseudomorph grains of biotites (including weathering products) were hand-picked from four horizons of a soil profile and from underlying granitic saprolite from the experimental Breuil-Chenue site (France).

Unexpected behaviors of U and Th nuclides were recorded from these samples. An unambiguous leaching of ^{232}Th occurs during the weathering of biotite, while reduced U release relative to Th was observed, implying an efficient redistribution of U between the primary mineral and weathering products within the pseudomorphs. The measured U-series activity ratios reflect a regular and self-consistent pattern evolution. However, the "U-series-derived-weathered-stage" is not always coherent with the weathering features of major elements and/or with the location of the samples within the soil profile. For instance, biotite from the saprolite displays U-series activity ratios typical of significantly weathered samples, while major elements present rather limited signs of weathering. These results suggest an incongruent leaching of U and Th isotopes and suggest that U- and Th-series nuclides probe some water-mineral interactions that occur before macroscopic mineral tansformation.

Using an open-system leaching model, coupled ($^{234}U/^{238}U$), ($^{234}U/^{230}Th$), and ($^{226}Ra/^{230}Th$) disequilibria measured from the samples allow us to calculate a weathering duration range of 6 to 52 ka for most weathered samples of this soil profile. The biotite weathering rate deduced from these data ranges from 7.8×10^{-17} $mol.m^{-2}.s^{-1}$ to 6.5×10^{-16} $mol.m^{-2}.s^{-1}$, which is consistent with the range of field rates previously reported. This rate was compared to the weathering rate of biotites induced by the substitution of vegetation occuring 35 years ago in a nearby soil profile, which was about 2 - 3 orders of magnitude higher than the long-term rate reported above. This feature is perfectly consistent with the decrease in the weathering rate with time that was previously widely documented but that still remains debated. Our results allude to a valuable use of U-series isotopes for mineral-weathering field rate determination and report a decrease in silicate weathering rates over long- (10 000s of

years) and short-term (10s of years) weathering events recorded from the same site. The results show that short term laboratory experiments can be representative of field processes, and suggest that some forms of mineral weathering reactivation, similar to that observed during laboratory experiments, may naturally occur in soils in response to high frequency perturbation processes such as land cover change.

Keywords: biotite, field weathering rate, U-series

1. Introduction

Concerns regarding climate change and soils sustainability have urged scientists to better understand rates of weathering. Indeed, such chemical reactions can regulate atmospheric CO_2 concentration (Berner et al., 1997; Gaillardet et al., 1999) or neutralize acid rain (Drever and Hurcomb, 1986) through the consumption of carbon and/or protons. They can also affect soil fertility. For instance, mica weathering has been intensively studied, as mica is a source of nutrients essential for plant growth, including potassium, magnesium and iron (Hinsinger et al., 1992; Leyval et al., 1991; Martin et al., 2010; Turpault and Trotignon, 1994). Over recent decades, numerous studies have focused on determining mineral weathering rates through either short-term laboratory experiments or long-term field studies. These studies clearly demonstrate the time dependence of the weathering rate, with short-term laboratory rates generally being several orders of magnitude faster than long-term rates (Taylor and Blum, 1995; White et al., 2003; Maher et al., 2004; White and Buss, 2014, Buss et al., 2017). The cause of this discrepancy remains highly debated (e.g., Hochella and Banfield, 1995; Maher et al., 2006a, 2009; Hellman et al., 2012; White et al., 2017). One of the difficulties associated with this puzzle may arise from the reduced value and precision of long term rate determination, which relies on dissolved fluxes being exported by rivers and/or aquifers (e.g., Clow and Drever, 1996) or on change in regolith composition (e.g., White, 2002), implying the deconvolution of a specific mineral weathering among several others. A lack of "mid-term" data, i.e., on the 10s or 100s of years scale, also prevents the precise determination of the time dependency of the weathering rate equation, which would heavily constrain kinetic and therefore involved mechanisms.

U-series nuclides have previously been used to determine weathering rates in regoliths and soils over various time scales (Chabaux et al., 2003a, 2003b, 2013; Dequincey et al., 2002; Dosseto et al., 2008, 2012; Keech et al., 2013; Ma et al., 2010, 2012, 2013; Pelt et al., 2008; Rihs et al., 2011; Suresh et al., 2013, Gontier et al., 2015; Ackerer et al., 2016; Schoonejans et al., 2016 , see also Chabaux et al. (2008), and Vigier and Bourdon (2011) for recent reviews). The use of these nuclides as weathering chronometers is based on chemical and physical fractionation that occurs between a parent and its daughter nuclides during weathering processes, leading to a radioactive disequilibrium. The evolution of the weathered material composition during weathering is therefore modeled as the continuous

loss and gain of nuclides (precipitation/adsorption from atmospheric deposition and/or illuviation) in addition to radioactive decay. According to this open model, the disequilibrium between U-series nuclides evolves over time until a steady state is reached. The amount of time required to reach this steady state depends on the ratio between the various input, leaching and radioactive decay rates. During this period, the extent of U-series disequilibria records the amount of time elapsed since the inception of the loss and/or gain process, i.e., the inception of parent material weathering. The matching of the half-lives of U- and Th-series nuclides, i.e., 5 y to 247 ky, and the timescales of pedogenic and weathering processes render these nuclides particularly suitable for inferring the time constants of element transfers within soils or saprolite layers. Dosseto et al. (2014) used the U-series derived weathering ages of bulk sediments to indirectly determine catchment-wide mineral-specific weathering rates. Even more recently, Dosseto et al. (2019) investigated the use of separated biotite and quartz to infer the mineral dissolution rates as well as the regolith production rate. Except this recent study, the potential for U-series to determine the long-term weathering rate of a specific mineral remains largely unexplored.

In the present work, we investigate a new application of U series chronometer to ascertain the long-term biotite weathering rate within a soil profile. Biotite was chosen among common other silicate minerals in view of its generally high U concentration. For this purpose, U- series disequilibria were measured in several biotite grains extracted from a granitic soil profile previously studied at the bulk scale.

2. Material and methods

2.1 Site location

Sand-sized biotite grains were sampled from a soil profile located in the Breuil-Chenue forest (Morvan Mountains, 47°18'N-4°5'E, 638 m, France) (Fig. 1). This experimental site was established by the Institut National de Recherche Agronomique (INRA) in 1976 and belongs to the SOERE FORET and ANAEE network (www.gip-ecofor.org/f-ore-t/reseau). Mean annual air temperature and precipitation levels are 9 °C and 1280 mm respectively (Calvaruso et al., 2009). The native vegetation is composed of 150-year-old forest dominated by beech trees (*Fagus sylvatica* L). The bedrock is composed of coarsely grained facies of "Pierre qui Vire" leucogranite (Seddoh, 1973) with a mineralogical composition of 34 % quartz, 24 % K-

feldspar, 31 % albite, 9 % muscovite, 1.2 % biotite, 0.5 % chlorite and accessory minerals (Mareschal et al., 2015). Soils that have developed over this bedrock are acidic (pH range: 4.17-4.96, Rihs et al., 2016), well drained, and classified as Typic Dystrochrept with depths ranging from 120 to 140 cm. Mineralogical and physico- chemical descriptions can be found in Mareschal (2008), Mareschal et al. (2010; 2015) and Gontier et al. (2015). It should be noted that some residual gravels (grain size > 2 mm) of granite are still present throughout the entire soil profile (from 17 to 31 $\%_{wt}$ in the different soil layers, Mareschal, 2008). The late breakdown of the residual granite block can therefore release fresh biotite grains to the shallow soil layers. Two major forms of ongoing mineralogical transformation were identified: i) close to the bedrock, biotite and albite are transformed into kaolinite and gibbsite, and ii) in the surface layers, remaining biotite and muscovite are transformed into vermiculite and smectite with the precipitation of aluminum hydroxides in their interlayer sheets (Mareschal, 2008).

2.2 Mineral separation and treatments

Biotite grains were extracted from the following soil layers: 20-30 cm, 110-120 cm, 120-130 cm and 120-140 cm throughout a joint study (Voinot 2012). Aliquots of the same samples (except for the 120-140 cm sample) were analyzed in both studies. The grains were manually hand-picked from the bulk soil, except for the 20-30 cm horizon, from which biotite grains were extracted from the 50 - 200 µm and 0.2 - 2 mm soil fractions. Additional magnetic separation was performed using a magnetic sector and vibrator (AA DYNA-MITE Electric vibrator 230V 50Hz, 10VA). No heavy liquid was used during separation to avoid any contamination and/or leaching of the samples. Approximately 100 mg to 1 g of mineral was collected from each soil layer before being manually crushed in an agate mortar.

Biotite grains taken from a block of the granite sampled from saprolite at the bottom of the soil profile were also analyzed (corresponding to sample B_{0b} in Voinot 2012). The samples were recovered after crushing a macroscopically unaltered granite block. Two aliquots of the extracted grains were sampled for replicate analyses. In addition, this sample was treated to extract its interlayer and weakly bounded nuclides. The interlayer was extracted from roughly 50 mg of the sample with 40 ml of 1 M NaCl (pH 5.50) heated at 80°C over 7 days. After centrifugation, the supernatant was collected and acidified at pH < 2 before analysis. Fresh NaCl solution was added to the residual solid and extraction was repeated two more

times. U and Th concentrations were measured from the 3 sequentially extracted solutions. Major elements in the final residual solid treated with NaCl were analyzed after rinsing them with MilliQ water. Approximately 40 mg of this sample was also treated with 40 ml of a 0.2 M oxalate acid/ ammonium oxalate solution ($C_2O_4H_2$, $2H_2O$ - $(NH_4)_2C_2O_4$, H_2O) at pH 3 (Tamm, 1922, modified by Schwertmann, 1964). The purpose of this treatment was to extract amorphous and poorly crystallized Fe-Mn-Al oxy-hydroxides in addition to the sorbed fraction. The suspension was shaken over 4 hours in the dark, before being centrifuged at 5000 rpm for 5 min. The supernatant was collected for U, Th and Mg analyses.

2.3 Analytical techniques

^{238}U, ^{232}Th and ^{226}Ra contents were determined by isotope dilution along with U-Th isotopic compositions of the same powder digestion. Between 5 and 10 mg of the powdered samples were spiked with a purified ^{228}Ra and artificial ^{233}U-^{229}Th tracers calibrated with AThO rock - standard (Williams et al., 1992, Condomines et al., 1995). The dissolution procedure involved digestion in a distilled HNO_3-HF- $HClO_4$ acids mixture at 70°C before subsequent evaporation. The residues were then dissolved with HCl-H_3BO_3 acids at 100°C for 24 h, prior to subsequent evaporation. U-Th separation and purification procedures were carried out using the anion exchange chromatography techniques developed at the Laboratory of Hydrology and Geochemistry of Strasbourg (LHyGeS) (Dequincey et al., 2002; Granet et al., 2007; Pelt et al., 2008). Ra separation and purification were performed following the procedure developed by Pelt et al. (2013) and adapted from previous works by Chabaux et al. (1994) and Ghaleb et al. (2004).

Th concentrations and $^{232}Th/^{230}Th$ isotopic ratios were measured with a Thermo-Scientific Neptune multiple collector inductively coupled plasma mass spectrometer (MC-ICP-MS). Thorium concentrations were calculated from the measured $^{232}Th/^{229}Th$ ratios. A standard-sample-standard bracketing method was applied to correct raw data for instrumental mass bias using a mixture of IRMM035 standard solution and ^{229}Th spike (see Jeanbrun et al., 2012 for details). The $^{232}Th/^{230}Th$ isotopic ratio proposed by Sims et al. (2008) for the IRMM-035 standard was used (87873 ± 738 2SD) rather than the original certified value. The abundance sensitivity at 2 amu was ~30 ppb with an ~70-80 % transmission of the RPQ filter and yielded to ^{232}Th tailing on the ^{230}Th that was always valued

at less than 0.5 %. Therefore, no corrections were made for this negligible shift covered by analytical uncertainties.

The U and ^{226}Ra concentrations and $^{234}U/^{238}U$ isotopic ratios were measured by thermal ionization mass spectrometry (TIMS) using a Thermo- Scientific Triton mass spectrometer. The U concentrations were calculated from the measured $^{233}U/^{235}U$ ratios. The ^{226}Ra concentrations were calculated from the measured $^{226}Ra/^{228}Ra$ spiked ratios and the natural $^{226}Ra/^{228}Ra$ ratio estimated from the $^{230}Th/^{232}Th$ isotopic ratio assuming a radioactive equilibrium between ^{232}Th and ^{228}Ra activity, i.e., (^{228}Ra) = (^{232}Th). Due to the low percentage of ^{228}Ra arising from the sample in the sample-spike mixture (< 1 %), a shift from this assumed radioactive equilibrium would produce a negligible effect on the calculated ^{226}Ra concentration (e.g., less than 0.1 % for a 10 % shift away from the radioactive ^{232}Th - ^{228}Ra equilibrium).

Measurement accuracy and reproducibility were controlled by analyzing the HU1 uranium and IRMM-036 thorium standard solutions, the BE-N and BCR-2 rock- standards, and the isotopic ratio of the Ra spike measured before each sample series. The change in the Ra spike isotopic ratio observed over time due to ^{228}Ra decay was found to be consistent with theoretical decay within 0.6 % (2SD, N=19, 2012). Average ($^{234}U/^{238}U$) activity ratios and $^{232}Th/^{230}Th$ isotopic ratios measured in the HU1 and IRMM-036 standards were equal to 1.000 ± 0.007 (2 SD, N=24, 2012-2013) and 325,261 ± 2664 (2 SD, N=9, 2012), respectively, in agreement with previously published values for HU1 (Cheng et al., 2000; Delanghe et al., 2002) and IRMM-036 (Sims et al., 2008; Ma et al., 2012). Replicate analyses of BE-N and BCR-2 rock standards are reported in Table 1. These analyses yielded analytical uncertainty values (2SD, N = 9, 2012-2014) of 1 % for U and Th concentrations, of 1.5 % for ^{226}Ra concentrations, of less than 0.5 % for ($^{234}U/^{238}U$) ratios, of 1% for ($^{230}Th/^{232}Th$) ratios, of 1.5 % for ($^{230}Th/^{234}U$) ratios and of 2 % for ($^{226}Ra/^{230}Th$) ratios, in agreement with previously published values for BE-N (Govindaraju, 1994; Pelt et al., 2013; Carpentier et al., 2016) and BCR-2 (Sims et al., 2008; Koornneef et al., 2010; Carpentier et al., 2016; Cogez et al., 2018). The results highlight a slight ~7 ‰ enrichment in ^{230}Th compared to secular equilibrium and compared to data from Sims et al. (2008) and Carpentier et al. (2016), most probably related to the lack of ^{232}Th tailing correction before 2014 and to the uncertainty assigned to the IRMM035 bracketing standard. Total process blanks ranged from 60 to 120 pg for Th, ranged

196 from 2 to 90 pg for U and were valued at less than 0.05 fg for ^{226}Ra, thus representing less
197 than 1 ‰ of the analyzed samples.
198
199 Major elements in the mineral after interlayer extraction and Mg content in the oxalate
200 solution were measured by Inductively Coupled Plasma Atomic Emission Spectrometry (ICP-
201 AES) while U and Th concentrations in the extracted solutions were determined by
202 Inductively Coupled Plasma Mass Spectrometry (ICP-MS). The precision and accuracy of the
203 measured concentrations were tested by replicate analyses after alkali fusion with $Li_2B_4O_7$ of
204 the basalt BE-N, anorthosite AN-G, granite GS-N, dolerite WS-E, and diorite DR-N rock
205 standards (Govindaraju, 1994), yielding analytical uncertainties of 3 % and 10 % (2SD, N= 20
206 for each standard over the study period) for major and trace elements, respectively.
207
208 The N_2-BET specific surface area of the saprolite biotite sample of 6.0 ± 0.7 m^2/g, was
209 measured at the LIEC (Laboratoire Interdisciplinaire des Environnements Continentaux) in
210 Nancy, France, using a BEL Japan BELSORP-mini II instrument with nitrogen (purity > 99.995
211 %) as the adsorptive at 77 K.
212

213 # 3. Results

214 Previous analyses of the separated grains conducted by X-Ray diffraction and Scanning
215 Electron Microscopy reveal that these samples do not comprise pure biotite minerals alone
216 (Mareschal, 2008; Voinot, 2012). Mareschal (2008) studied several soil profiles from the
217 same site and highlighted the common presence of kaolinite, vermiculite and Fe-oxides in
218 biotite grains found in these soils. The presence of these weathering products is consistent
219 with a decrease in SiO_2/Al_2O_3 and K_2O/Al_2O_3 ratios observed from the deepest horizons to
220 the surface in the studied samples (Table 2). Mareschal (2008) also performed in- situ
221 microprobe measurements of sand-size biotite grains collected from the same site and
222 observed a decrease in the SiO_2 /Al_2O_3 ratio from pristine biotite (SiO_2 /Al_2O_3 = 1.8) to the
223 weathered area (SiO_2 /Al_2O_3 = 1.1) within the grains, corresponding to a kaolinization
224 process. In addition, a decline of K_2O content was observed, consistent with the widely
225 reported release of K during biotite weathering (e.g., Newman and Brown, 1966; Newman,
226 1969; Turpault et al. 1994; White 2002). Mareschal (2008) proposes that the weathering

products formed from an intragrain reprecipitation of the leached elements from weathered biotite. The separated grains therefore correspond to the pseudomorphosis of parent biotites, including weathering products retained within the unchanged volume and fabric of the parent minerals. Such pseudomorphic replacement of biotites by kaolinite has been previously well documented (e.g., White et al., 1998; 2002). The quantitative mineralogy, i.e., the mass fraction determination of each component in the grains, was quantified by Voinot (2012) through chemical analyses of the grains (reported in Table 2), differential thermal analyses, chemical analysis of each mineral and of XRD data following the methodology developed by Fichter et al. (1998) and Turpault et al. (1998). Normative calculations using standard minerals allow to determine the fraction of each mineral by resolving a system of simultaneous linear equations based on the chemical content of a particle size fraction on one hand and from the corresponding element content of single minerals on the other. Between 7 and 17 % of quartz was identified in the analyzed grains, representing an imperfect biotite grain separation. Scanning Electron Microscopy also reveals some traces of accessory minerals such as Ti oxides (< 2 %) and chlorite (< 1 %) (Voinot, 2012). In view of the low abundance of these accessory minerals or of the low U concentrations generally observed in quartz (0.1 - 1 ppm, Bosia et al., 2018; Dosseto et al., 2019), these impurities are not expected to significantly impact U-series activity ratios measured in the separated grains, wherein measured U concentrations range from 31 to 65 ppm. With a view to consider the amount of weathered biotite present within the analyzed grains, the proportion of remaining biotite and the weathering products were therefore recalculated from the results of Voinot (2012) without quartz contribution, i.e.: biotite and weathering products proportions were normalized to 100 % after subtracting quartz proportion. According to this calculation, samples collected from deep soil layers are composed of about 60 % biotite (quartz excepted) while fine grains from the surface soil layer (20-30 cm 50-200 µm) do not hold more than 28 % (quartz excepted) of biotite anymore (Fig. 2). Consistent with the decline of K_2O content mentioned above, the remaining amount of biotite calculated strongly correlates with the K_2O concentrations and K/Fe, K/Al or Si/Al ratios (not shown). All of these parameters therefore represent equivalent proxies for the weathering state of biotite grains.

3.1. U-series disequilibria

U, Th concentrations and activity ratios are reported in Table 3. Replicate analyses of biotite grains from the granitic saprolite show different U and Th concentrations (differences of 5 % and 10 %, respectively while analytical uncertainties are 1 %). These replicated analyses were not performed on aliquots of a single powder sample, but on aliquots of non-crushed biotite grains, and they therefore highlight the heterogeneity of U and Th concentrations in these minerals. However, ($^{234}U/^{238}U$), ($^{230}Th/^{234}U$) and ($^{226}Ra/^{230}Th$) activity ratios of the two subsamples are identical within analytical uncertainty, emphasizing the significance of the measured U-series disequilibria independent of probable initial U heterogeneity.

During water-rock interactions and therefore weathering processes, U-series nuclides are expected to fractionate. Detailed reviews can be found in Chabaux et al. (2008), or Vigier and Bourdon (2011). In brief, in an oxic environment, U is usually highly mobile while Th is known to be very insoluble. The mobility of Ra is strongly controlled by redox state but is generally higher than that of Th. In addition, fractionation between ^{234}U and ^{238}U isotopes may occur due to alpha-recoil process (Kigoshi, 1971). Therefore, the following features are anticipated during weathering process: U and Ra loss, Th immobility, ($^{234}U/^{238}U$) and ($^{226}Ra/^{230}Th$) ratio decline concomitant with an increase in the ($^{230}Th/^{234}U$) ratio. In the study biotite grains, U and Th concentrations cover a broad range through the profile (30 to 65 ppm and 100 to 338 ppm respectively). In the shallowest horizon (20-30 cm), concentrations in the coarse-size fraction (> 200 µm) are significantly higher than those in the fine-size fraction (50- 200 µm). U contents do not show a clear trend with the decrease in K content while Th contents decrease significantly (Fig. 3). Consequently, the evolution of the U/Th ratio is not correlated with weathering pattern determined from major elements and mineralogy (Fig. 4a). This ratio is, in contrast, strongly correlated with Ti content (Fig. 4b).

($^{234}U/^{238}U$), ($^{230}Th/^{234}U$) and ($^{226}Ra/^{230}Th$) activity ratios range from 0.73- 0.93, from 1.04 – 1.14 and from 0.67 – 0.91, respectively (Table 3). Despite an overall increase in the disequilibrium extent observed toward the surface, i.e., the deepest soil samples are closer to the secular equilibrium than samples from the topsoil layer, grains extracted from the granitic saprolite are inconsistent with this pattern of evolution, as they exhibit some of the largest disequilibria values (($^{234}U/^{238}U$) = 0.76, ($^{230}Th/^{234}U$) = 1.10 and ($^{226}Ra/^{230}Th$) = 0.76). Similarly, the two samples separated from the same topsoil layer (20-30 cm) show contrasting disequilibria (($^{234}U/^{238}U$) = 0.73 and 0.79 in fine < 200 µm and coarse > 200 µm fractions, respectively), highlighting the size-dependence of U-series disequilibria and

weathering states. Such an irregular evolution of sample compositions with depth was also noticeable from the quantitative mineralogy of grains (Fig. 2). For instance, the amount of remaining biotite is significantly higher in the shallow coarse sample (20-30 cm > 200 µm) than in samples from the deepest soil layers. In granitic weathering profiles, such inversion of weathering polarity can be easily explained. Indeed in arenas the large-scale view of upward vertical polarity observed from fresh rock to the topsoil can be disturbed at the outcrop scale through the preferential weathering of fractured zones (Meunier, 2005). In addition, the remanence of large granite gravel throughout the entire soil profile implies the release of relatively fresh (or at least less weathered) minerals in the surface soil layers. The coarse > 200 µm sample from the 20-30 cm layer may reflect such origin while the fine < 200 µm (more weathered) fraction may have been inherited from the deeper granitic bedrock weathering front. According to this assumption, fine and coarse fractions of the 20-30 cm soil layer may therefore simply reflect different weathering durations. This implies that any time determination made for these samples cannot be related to the velocity of weathering front migration. Such inversion/disturbance of weathering polarity was not observed in previous analyses of the corresponding bulk soil samples (Gontier et al., 2015), most likely due to the analysis of the mere fine earth fraction (< 2 mm) and to the greater mass of the sample used for bulk analyses, which is expected to reduce small-scale heterogeneity. More unexpected, the U-series disequilibria are neither consistent with the weathering state of the grains based on the K/Fe ratio or on the remaining amount of biotite (Fig. 5). As for the relationship with depth, biotite extracted from the saprolite and the coarse shallow sample (20-30 cm > 200 µm) do not follow the observed trend.

Nevertheless, all U-series activity ratios demonstrate regular and self-consistent evolution when localization or weathering state based on major elements are not considered (Fig. 6). The observed decline in the ($^{234}U/^{238}U$) ratio closely follows the increase in the ($^{230}Th/^{234}U$) ratio and the decrease in the ($^{226}Ra/^{230}Th$) or the ($^{226}Ra/^{238}U$) ratios. Likewise, the decrease in the ($^{234}U/^{238}U$) ratio is anti-correlated with the increase in the ($^{238}U/^{232}Th$) ratio (Fig. 7a). The isochron ($^{230}Th/^{232}Th$) vs ($^{238}U/^{232}Th$) diagram also shows a regular evolution of the samples compositions, albeit below the equiline (Fig. 7b). The nuclides mobility implied by these variations is discussed below (section 4.1).

3.2 Selective treatments of the saprolite biotite

The major element contents in the residual mineral after interlayer extraction are reported in Table 2. The significant decrease in K_20 concentration (7 to 4 wt%) and the concurrent increase in Na_2O concentration(0.7 to 6.2 wt%) suggest the exchange of K by Na and confirm the efficient extraction of the interlayer. U and Th percentages extracted during the 3 successive extractions are reported in Table 4. The total amount of U and Th extracted is limited (~1 and 0.2 % of the total U and Th) and a rapid decrease in the proportions of U and Th extracted is observed over the 3 successive extractions, ranging from 0.7 to 0.05 % for U and from 0.15 to 0 % for Th.

The amount of U and Th adsorbed and/or associated with amorphous Fe-Mn-Al oxy-hydroxides was also found to be low: 2 % of the total U and 4 % of Th (Table 4). Despite the previously reported ligand-promoted dissolution of biotite by oxalate solutions (e.g., Haward et al., 2011), the low level of Mg release (0.4 %) precludes significant biotite dissolution during such extraction.

4. Discussion

4.1 Origin of U/Th variability

Patterns of U and Th content variability observed from the samples described above (Fig. 3 and 4) cannot be explained by usual weathering processes during which U is usually highly mobile while Th is known to be very insoluble (Chabaux et al., 2008; Vigier and Bourdon, 2011). A decrease of U/Th ratio is therefore expected during weathering process, in contrast with the evolution of the U/Th ratios observed in the analyzed samples (Fig. 4a). Issues concerning initial heterogeneity and/or the removal of typically immobile elements (e.g., Th and Ti) to explain the observed trends therefore arise in order to further model the observed U-series disequilibria. Heterogeneous initial U/Th ratios can indeed produce a trend similar to that observed along the equiline in the ($^{230}Th/^{232}Th$) vs ($^{238}U/^{232}Th$) isochron diagram (Fig. 7b). However, in this diagram, whatever the initial positioning of the sample, the observed shift from the equiline involves an increase in the U/Th ratio and/or a decrease in the ($^{230}Th/^{232}Th$) isotopic ratio. An increase in the U/Th ratio due to a gain of U in these samples is highly unlikely in view of several of the following features: i) U content does not

significantly increase in samples with low amount of remaining biotite (or low K content) (Fig. 3); ii) the concurrent decrease in Ti and increase in U/Th (Fig. 4b) would imply a correlated loss of Ti with gain of U; iii) the 20-30 cm (50-200 µm) sample presents the highest U/Th ratio but the lowest ($^{234}U/^{238}U$) activity ratio (= 0.73). A gain of ^{238}U in this sample would therefore imply a lack of ^{234}U gain (e.g., 30 % of gained ^{238}U in this sample would require a ($^{234}U/^{238}U$) input ratio of as low as 0.3); iv) the extraction of exchangeable cations using NaCl and of amorphous and poorly crystallized Fe-Mn-Al oxy-hydroxides using oxalate ammonium solution from the saprolite biotite with a high U/Th ratio, i.e.: sample that could be suspected to have gained some U, yielded a recovery value of less than 1 % of U for the exchangeable fraction and no more than 2 % of U for the amorphous oxy-hydroxides fraction, precluding the presence of significant amount of adsorbed U. A loss of Th (either ^{230}Th relative to ^{232}Th or ^{232}Th relative to ^{238}U or both) is therefore mandatory to explaining the positioning of the samples below the equiline in the ($^{230}Th/^{232}Th$) vs ($^{238}U/^{232}Th$) diagram. The ongoing decline in Th content observed in the most weathered samples (Fig. 3) denotes ^{232}Th loss, but Th leaching was also independently assessed for ^{230}Th relative to ^{238}U (section 4.3). Such loss implies a concurrent loss and/or heterogeneity of Ti to explain the U/Th vs Ti relationship (Fig. 4b). As suggested by the variability of U and Th contents in replicates of the saprolite biotite sample, some heterogeneity of the trace element contents in the study samples can be suspected, and the presence of Ti-oxides in some of our samples (Fig. 2) strongly supports this doubt. Accordingly the Ti contents of the study grains are inconsistent with major elements (SiO_2/Al_2O_3 or K_2O/Fe_2O_3 ratios for instance) and mineralogy. In addition, if a Ti initial homogeneous content and its immobility was assumed, the decrease of TiO_2 content from 2.4 % (in the saprolite biotite) to 1.3 % in the fine 20-30cm (50- 200µm) sample would imply the precipitation of about the same mass of secondary, Ti-depleted material than primary material (i.e. the mass must be multiplied by 2). This appears highly unlikely within a grain where the volume and fabric of the primary biotite mineral remain preserved. In contrast, the release of Ti from the crystallographic structure of biotites, through chemical weathering was previously reported (Cornu et al., 1999; Taboada et al., 2006). Hence, the use of Ti as reliable weathering proxy is not relevant in these samples.

Based on all these features, and despite the potential presence of slight initial heterogeneities, the observed U and Th contents variability seems therefore most likely

attributable to a preferential loss of Th relative to U Several previous studies have identified Th mobility in soil, usually linked to organic matter complexation (Dosseto et al., 2008; Rezzoug et al., 2009; Rihs et al., 2011; Keech et al., 2013; Gontier et al., 2015, Dosseto et al., 2019). In the present study, however, a similar Th mobility is observed from samples positioned at the bottom of the soil profile as well as at the surface. Such Th mobilization observed across the entire soil profile was already highlighted from corresponding bulk samples (Gontier et al., 2015) despite a significant decline in C organic content in seepage soil solutions with depth (Jaffrain, 2006; Cornelis et al., 2010) as well as in soil layers (Marechal et al., 2013; Rihs, Gontier et al., 2016). Alternatively, the relationship between U/Th and Ti (Fig. 4b) could suggest a removal of solid Ti- and Th- rich nanoparticles from accessory minerals. However, such an assumption cannot explain the preferential removal of ^{230}Th relative to ^{238}U (section 4.3) as both nuclides are expected to be located within the same mineral fraction. These results echo various recent works that report Th mobility across different contexts where organic complexation appears to be precluded. For instance, Bosia et al. (2018) showed that zircons from Gandak River sediments (Himalaya) have undergone a loss of both ^{230}Th and ^{232}Th isotopes. Additional in-situ SIMS analyses of the Gandak River samples demonstrate that the Th depletion is not restricted to the grain surface, but instead continues 15-20 µm below the mineral surface while the (^{234}U/^{238}U) ratios remain equal to 1 (Bosia, 2016). Menozzi (2016) and Dosseto et al. (2019) also reported a significant leaching of ^{230}Th from quartz sampled in both granitic and sandstone saprolites at a depth of 2.5 m and in apparently pristine bedrocks (New South Wales, Australia). In contrast, a gain of ^{232}Th (as well as U) was observed by these authors in the biotite separated grains from the granitic profile, highlighting, if needed, the influence of external-to-the-mineral factors on nuclides behavior in weathering profiles. Rihs et al. (2011) showed that the leaching constants of both Th isotopes in deep soil layers of the Strenghbach catchment (Vosges, France) are at least two orders lower than those observed in the shallowest soil layers where organic complexation has been identified. Clearly, these results suggest that the mechanism(s) of Th mobilization observed in weathering environments remain(s) poorly understood and need(s) further investigations.

413

414 **4.2 Weathering signal recorded by U-series versus major elements.**

415 During water-rock interaction, U-series nuclides fractionation usually produces radioactive
416 disequilibria in the U-series decay chain (Chabaux et al., 2008). Yet, major elements and U-
417 series disequilibria data are opposing in the saprolite biotite and coarse 20-30 cm (> 200 µm)
418 samples. These samples are indeed significantly out of radioactive equilibrium while major
419 elements contents and mineralogical analyses suggest only minor patterns of weathering
420 evolution (Fig. 5). For instance, saprolite biotite grains comprise 92 % of remaining biotite
421 and 8 % of quartz (or 100 % of biotite with quartz excepted), without traces of secondary
422 minerals (Fig. 2) and the coarse 20-30 cm (> 200 µm) grains contain the second highest
423 amount of remaining biotite (75 %, quartz excepted). Yet, the low ($^{234}U/^{238}U$), ($^{230}Th/^{238}U$)
424 and ($^{226}Ra/^{230}Th$) ratios observed in these samples (Table 3) imply a considerable removal of
425 ^{234}U, but also of ^{230}Th and ^{226}Ra, thus involving significant water-mineral interactions not
426 detected by major elements. Two mechanisms of non-stoechiometric nuclide removal could
427 be assumed from the biotite: i) a direct ejection of daughter nuclides by alpha-recoil or ii) a
428 leaching from the mineral interlayer. Owing to the large size of the separated grains (> 200
429 µm), no models recently developed to estimate the alpha-recoil loss fraction (Depaolo et al.,
430 2006, Maher et al., 2006b; Bourdon et al., 2009) predict a rate of ejection higher than 0.01,
431 thus failing to explain a ($^{234}U/^{238}U$) ratio as low as 0.76 – 0.79. In addition, Depaolo et al.
432 (2006) compare the timescales of ^{234}U alpha-recoil and mineral dissolution processes as
433 follow:

434

435 $$\frac{\tau_{recoil}}{\tau_{dissolution}} = \frac{R \times M}{^{234}\lambda \times L \times \rho} \qquad [1]$$

436

437 where τ_{recoil} and $\tau_{dissolution}$ denote the timescales of alpha-recoil and mineral dissolution
438 processes, respectively, R denotes the dissolution rate of the mineral (in $mol.m^{-2}.s^{-1}$), M
439 denotes the molar mass of biotite ($g.mol^{-1}$), λ_{234} denotes the decay constant of ^{234}U (s^{-1}), L
440 denotes the alpha-recoil distance of ^{234}Th (m) and ρ denotes the mineral density (g/m^3).
441 Using L = 30 nm (Maher 2006b), ρ = 2.97 $g.cm^{-3}$ (Turpault and Trotignon, 1994), M = 445
442 $g.mol^{-1}$ and R the range of biotite field weathering rates reported by White and Brantley
443 (2003) as $1.3.10^{-16}$ – $7.9.10^{-15}$ $mol.m^{-2}.s^{-1}$, this dimensionless number ranges from 7 to 445,

444 indicating that the timescale for ^{234}U recoil is one or two orders of magnitude longer than
445 that of the mineral's dissolution. This indicates that the mineral would dissolve before the
446 alpha-recoil process could significantly deplete the ^{234}U isotope from this mineral and
447 therefore precludes significant ^{234}U recoil from these minerals.
448 Alternatively, leaching from the mineral interlayer (hypothesis ii above) might be assumed.
449 In view of the phyllosilicate structure of biotite, a significant implementation of ^{234}U in the
450 mineral interlayer space by alpha-recoil can be expected. Approximately 1.2 Ma after the
451 mineral's formation, all ^{234}U present in the mineral ensues from ^{238}U decay and would
452 therefore be located in the mineral following an alpha-recoil implementation. Based on a 2:1
453 sheet and an interlayer thickness of 0.66 nm and 0.34 nm respectively (Dahl, 1996), simple
454 geometric consideration predicts that roughly 30 % of the ^{234}U produced through ^{238}U decay
455 would be located within the interlayer. Assuming such amount, the ($^{234}U/^{238}U$) ratio
456 measured from the saprolite biotite (= 0.76) would imply that the quasi-totality of interlayer
457 ^{234}U was leached out. The interlayer extraction of this sample indeed confirms a low amount
458 of interlayer U (< 1 % of U) that could be consistent with a previous depletion. However,
459 initial K_2O content (7.8 %) within this sample was only slightly lower than in the
460 unweathered mineral (9.4 %) determined by Mareschal (2008). In contrast, during interlayer
461 extraction, a large amount of K was, as expected, removed (K_2O content dropped to 4 %
462 after NaCl treatment). A previous leaching of ^{234}U from the interlayer would therefore imply
463 a nearly full removal of ^{234}U without K release. Such disconnected fluxes could appear
464 dubious. However, Wan et al. (2017) suggest that preferential dissolution from weaker
465 surface defects on basal biotite surfaces produces a path for CO_2 entry to the mineral
466 interlayer more likely than simple diffusion from the edges. Such a process allows for
467 mobility of elements from and out of the interlayers without concurrent K mobility. In
468 addition, the U-series weathered-signature of the saprolite and the coarse 20-30 cm > 200
469 µm samples are actually consistent with their high $\delta^{11}B$ isotopic composition (-26.8 and -23.5
470 ‰ respectively while the value measured from the unweathered biotite is -31 ‰) reported
471 by Voinot (2012). This author suggests that B isotopic composition evolves faster than
472 mineral transformation and emphasizes nanoscale mechanisms that control B release. U-
473 series, as B isotopes, therefore seem able to trace early weathering reactions before major
474 elements and/or mineralogical proxies. The difference observed here between major and
475 trace element signatures raises issues concerning the stoichiometric release of trace

elements during weathering. Trace elements are widely used to refine conditions of water-rock interactions, e.g., Sr (Bullen et al., 1997, White 2017), B (Lemarchand et al., 2012), Li (Millot et al., (2010), and U (Maher et al. 2004, 2006a,b), and the assumption of the stoichiometric release of these elements during mineral weathering constitutes a key point. Several studies have addressed this issue but have generated contradictory results for non-radiogenic as well as radiogenic isotopes. For instance, the stoichiometric or non-stoichiometric release of non-radiogenic ^{86}Sr seems to depend on the mineral considered: K-feldspar (Bullen et al., 1997; Brantley et al., 1998) labradorite or biotite (Taylor et al., 2000a, b). Similarly, Olander and Eyal (1990) demonstrate a non-stoichiometric release of ^{238}U and ^{232}Th from monazite over a 6.8-year experiment while Andersen et al. (2009) suggest a congruent dissolution of granite minerals with respect to ^{238}U. For radiogenic isotopes, Bullen et al. (1997) report a non-stoichiometric release of ^{87}Sr while Andersen et al. (2009) highlight transient features of the non-stoichiometric release of ^{234}U. This transient issue, also identified by Brantley et al. (1998) for Sr isotopes, is fundamental, as most of the reported results arise from experimental studies, i.e., short-term relative to a natural weathering timescale. In contrast, the results of the present study emphasize the early and preferential release of U-series nuclides relative to the major element over a natural weathering timescale.

4.3. Long-term weathering rate of the biotite

To estimate the duration of mineral weathering, an open model was used (Vigier et al., 2001) where decay and leaching are considered as follows:

$$\left.\begin{aligned} \frac{d^{238}U}{dt} &= -(\lambda_{238_U} + k_{238_U})^{238}U \\ \frac{\mathrm{d}\ ^{\mathrm{n}}\mathrm{N}}{\mathrm{dt}} &= -\left(\lambda_{\mathrm{n}} + \mathrm{k}_{\mathrm{n}}\right)^{\mathrm{n}}\mathrm{N} + \lambda_{\mathrm{n}-1}{}^{\mathrm{n}-1}\mathrm{N} \end{aligned}\right\} \quad [2]$$

where ^{n}N stands for the number of ^{234}U, ^{230}Th or ^{226}Ra atoms, and ^{n-1}N the abundance of the corresponding parent nuclide. k_n and λ_n (y^{-1}) are the leaching and decay constants of the nuclide ^{n}N, respectively.

No gain of nuclides was used in this model as justified for U in the above section (4.1). For ^{230}Th and ^{226}Ra, the high content of these nuclides in the samples (resulting from high U content i.e., 40-50 ppm) renders them much less sensitive to potential gains. Such a model is consistent with the commonly observed mechanism of biotite alteration to kaolinite or vermiculite through epitaxial weathering without external gain (White, 2002). The 120-140 cm sample, characterized by the closest-equilibrium state, was used as initial material. Owing to uncertainties related to the coarse 20-30 cm (> 200 µm) and saprolite samples described above, the two samples were discarded for the fit and data from the 120-140 cm, 120-130 cm, 110-120 cm and the fine 20-30 cm (< 200 µm) samples only were fitted by the model. We solved the set of model equations (2) using the differential equation solver (ode45) available through Matlab® commercial software. We randomly selected 500 sets of initial k_n values in the range 10^{-6} to 10^{-3} y^{-1} and solved the differential equations over 500 ky. Each initial set of leaching constants was adjusted using the Matlab® lsqnonlin function to fit the measured ($^{234}U/^{238}U$), ($^{230}Th/^{234}U$) and ($^{226}Ra/^{238}U$) ratios of each sample. In view of uncertainties related to the homogenous initial U content discussed above, the evolution of U concentrations in the samples was not used as a model parameter. Finally, only the sets of parameters matching the measured ratios within $\pm$ 2SD uncertainty levels and yielding k_{234}/k_{238} ratios lower than 5 were retained. The range of solutions describing the measured data is reported in Table 5. Radium presents the highest leaching constant ($k^{226}Ra \approx 10^{-4}$ y^{-1}) within a very narrow range consistent with the short half-life of this nuclide. As one striking feature of these solutions, leaching constants of ^{230}Th are lower than those of ^{234}U but are higher than those of ^{238}U ($k^{238}U/k^{230}Th < 1$, Fig. 8). These results obtained without any constraints on ^{230}Th mobility are fully consistent with the preferential leaching of ^{232}Th relative to ^{238}U, highlighted above.

The amount of time required to evolve from the initial sample (120-140 cm) to the most out-of-equilibrium sample positioned in the shallowest soil layer (20-30 cm, < 200 µm) ranges from 6 to 52 ky. The two extreme models, i.e., leading to a duration of 6 and 52 ky respectively, are represented in Fig. 6, along with the measured data. While excluded from best-fit optimization, the 20-30 cm (> 200 µm) and saprolite biotites are also reported in the figure, and were found to be consistent with the retained models.

For the two reported models, the evolution of the ($^{238}U/^{232}Th$) and ($^{230}Th/^{232}Th$) ratios can be reproduced assuming a leaching of ^{232}Th (Eq. 2 applied to ^{232}Th). Leaching constants of ^{232}Th yielding the best-fit to the data are reported in Table 5, and corresponding models are reported in Fig 7a and 7b. The required $k^{232}Th$ leaching constants are higher than those of $k^{238}U$ and $k^{230}Th$.The evolution of the ($^{230}Th/^{232}Th$) vs ($^{238}U/^{232}Th$) ratios observed across all of the samples can be satisfactorily described with both models (Fig. 7b). In contrast, the models failed to reproduce the ($^{234}U/^{238}U$) vs ($^{238}U/^{232}Th$) ratios of the 20-30 cm (> 200 µm) and saprolite samples and are even questionable for the 110-120 cm sample (Fig. 7a). However, a slight change in the initial ($^{238}U/^{232}Th$) ratio (e.g., 0.37 instead of 0.48) allows for the reproduction of the ($^{234}U/^{238}U$) vs ($^{238}U/^{232}Th$) ratios of the saprolite and 110-120 cm samples while a minor change in the ($^{230}Th/^{232}Th$) vs ($^{238}U/^{232}Th$) pattern was induced by this lower initial ($^{238}U/^{232}Th$) ratio (Fig. 7b). These results reinforce the hypothesis of potential initial U/Th heterogeneity in the biotite samples presented above, but demonstrate the low sensitivity of the so-called ($^{230}Th/^{232}Th$) vs ($^{238}U/^{232}Th$) isochron diagram to such heterogeneity. Figure 7b shows that the variation of the ($^{230}Th/^{232}Th$) is, to first order, driven by time rather than initial U/Th ratio. Yet, the models reported in Fig. 6, the corresponding elapsed time, and therefore the deduced weathering rates calculated below are completely independent of this heterogeneity.

The biotite weathering rate was calculated from the minimum and maximum amount of time required for evolution from 110-120 cm to 20-30 cm (< 200 µm) samples (5.8 and 49 ky using models 1 and 2, respectively). The 120-140 cm sample, used as initial material in the U-series models, could not be used for weathering rate determination, as the fraction of the remaining biotite mineral was not resoluted in this sample. However, the 110-120 cm sample presents a very similar U-series signature (Fig. 6). The amount of dissolved mineral was calculated through the estimation of the biotite mass fraction remaining in the grains (Voinot, 2012), i.e., 60 % and 28 % in the 110-120 cm and 20-30 cm (< 200 µm) samples, respectively, (Table 3) assuming an isovolumetric weathering. The weathering rate, R, was then calculated as follows:

$$R = \frac{\frac{m_i - m_f}{M}}{T \times S} \qquad [3]$$

where m_i and m_f are the initial and final mass of the biotite per g of sample respectively, M is the molar mass of biotite, calculated from structural formulae of the studied biotite established by Marechal (2008) (455 $g.mol^{-1}$), T is the weathering duration determined by U-series models and S is the measured specific surface area (6 $m^2.g^{-1}$).

This calculation yields a weathering rate R ranging from 6.5×10^{-16} $mol.m^{-2}.s^{-1}$ (model 1) to 7.8×10^{-17} $mol.m^{-2}.s^{-1}$ (model 2). The isovolumetric weathering assumption may lead to an overestimation of the dissolved mass and thus to an underestimation of weathering rates. However, such isovolumetric weathering is a common feature observed in saprolites developed in tropical and temperate environments (White et al., 1998, 2002), and the calculated rates are fully consistent with field weathering rates of biotite previously reported from a variety of lithology and climatic regimes (Fig. 9). It should be noted that the highest rates reported in Fig. 9 for timespans of 10^4 and 3×10^5 y correspond to the tropical Rio Icacos Watershed (Puerto Rico) (White et al., 2002, Murphy et al., 1998; Buss et al., 2008). The rate calculated from model 1 in the present study was found to be similar to the rate derived from sedimentary chronosequences of the Rhône and Oberaar Glaciers (Swiss Alp) reported by Föllmi et al. (2009) (≈ 2×10^{-15} $mol.m^{-2}.s^{-1}$ over a 10 ky timespan, corresponding to rates based on the total mineral surface area rather than the edge surface to compare to the present and previously reported studies). These results demonstrate that U-series can provide a useful tool for long-term mineral rate determination, as suggested by Dosseto et al. (2014, 2019). Actually, the assessment of a long-term field mineral dissolution rate is difficult and is classically based on dissolved fluxes exported by rivers and/or aquifers or on changes in the regolith composition coupled with cosmonuclide-based denudation rate estimation (review given in White and Buss, 2014). Considerable uncertainties affect these approaches, hampering the resolution of long-standing assessments of the apparent discrepancy between laboratory and field weathering rates (Paces, 1983; Taylor and Blum, 1995; White and Brantley, 2003; Maher et al., 2004, 2009; Hellman et al., 2012; White et al., 2017). U-series disequilibria of regolith-separated minerals offer a new direct approach that could be applied to other common silicate minerals.

4.4. Comparison to short-term weathering rates

We previously studied nearby soil profiles from the same experimental site, where the native forest was partially clear-felled in 1976 and replaced with monospecific Oak and Douglas Fir stands (Rihs, Gontier et al., 2016). U- and Th-series disequilibria were measured from bulk soils developed under the native forest (as in the present study) and from the two replanted stands. We found that tree substitution (the change in specie as well as associated temporary soil denudation) had yielded a considerable dissolution of biotites in the soil under the replanted Oaks. The mean biotite weathering rate deduced from this recent substitution was found to be equal to 1.1×10^{-12} $mol.g^{-1}.s^{-1}$, corresponding to a value of 1.8×10^{-13} $mol.m^{-2}.s^{-1}$ with a specific surface area S = 6 $m^2.g^{-1}$. This rate is roughly 2 or 3 orders of magnitude higher than the long term rate calculated above from the same site without vegetation substitution but is consistent with the rate that could be extrapolated for a 35-year weathering period from the time-dependent relationship proposed by White and Brantley (2003) or from rates deduced from sedimentary chronosequences of the Rhône and Oberaar Glaciers at 140 and 270 y (Föllmi et al., 2009) (Fig. 9). This result is noteworthy as it probes a period of time, i.e., 35 years that is too long for laboratory experiments and too short for classical field, long-term studies, leading to a critical lack of data. This shows that short-term laboratory experiments can be representative of field processes, and suggests that mineral weathering reactivation, similar to what is observed in laboratory experiments, may naturally occur in soils, in response to perturbation, i.e., land cover change in the present case.

5. Conclusion

Long-term field weathering rate of biotite was determined using U-series disequilibria measured from several grains extracted from a granitic soil profile at different depths. The grains correspond to the pseudomorphosis of parent biotites, including weathering products retained within the unchanged volume and fabric of the parent minerals. The remaining parent biotite ranges from 100 % to 28 % in the study samples.

Despite potential initial U/Th content heterogeneities in the samples, the U-series activity ratios describe a regular and self-consistent pattern of weathering evolution. This weathering evolution however involves a significant loss of Th, highlighting that the mechanism of Th mobilization observed in weathering environments remains poorly understood and deserves further investigations. In addition, some samples show significant

U-series disequilibria while major element contents and mineralogical analyses show only minor signs of weathering. This discrepancy between the "U-series-derived- weathered - stage" and macroscopic features emphasizes a nanoscale mechanism that controls U-series nuclides release and suggests that these nuclides can trace early weathering reactions before major elements and/or mineralogical proxies.

An open-system model based on radioactive decay and leaching rates was applied to successfully describe ($^{234}U/^{238}U$), ($^{234}U/^{230}Th$), and ($^{226}Ra/^{230}Th$) disequilibria evolution and to infer the amount of time required for the less weathered sample, located in deep soil layers to evolve into the most out-of-equilibrium sample found in the shallowest soil layer. The model demonstrates the low sensitivity of the ($^{230}Th/^{232}Th$) vs ($^{238}U/^{232}Th$) diagram to U/Th initial heterogeneity in the samples. The biotite weathering rate was deduced from the determined duration and the amount of mineral dissolved. This latter was calculated through an estimation of the biotite parent mineral remaining in the analyzed grains (Voinot, 2012). The deduced weathering rate ranges from 7.8×10^{-17} mol.m^{-2}.s^{-1} to 6.5×10^{-16} mol.m^{-2}.s^{-1}, which is perfectly consistent with long-term field weathering rates of biotite previously reported. These results demonstrate that U-series disequilibria of regolith-separated minerals offer a useful and direct means of determining long-term weathering rates. In addition, we previously showed that experimental vegetation substitution occurring 35 years ago close to the study soil profile spurred a considerable dissolution of biotites under Oak replaced stands (Rihs, Gontier et al., 2016). The substitution-induced weathering rate of the biotite measured under the replaced vegetation was found to be 2 or 3 orders of magnitude higher than the long-term rate obtained through the present study but is consistent with the rate that can be extrapolated from the time-dependent relationship proposed by White and Brantley (2003). These results document a decrease in silicate weathering rates from long- (10,000s of years) and short-term (10s of years) weathering events for the same site. They show that short-term laboratory experiments can be representative of field processes and suggest that some processes of mineral weathering reactivation, similar to that observed during laboratory experiments, may naturally occur in soils, in response to short-term perturbation such as land cover change.

Acknowledgements: The authors acknowledge the SOERE FORET and ANAEE networks, Arnaud Legout and the INRA-BEF (Biogéochimie des Ecosystèmes Forestiers) team for

managing the Breuil- SORE site and sampling and mineral separation, and René Boutin (LHyGeS) for conducting ICP analyses. The constructive comments of two anonymous reviewers helped to improve the manuscript. This work was financially supported by the INSU- Syster Program. This research is an EOST contribution.

References

Ackerer J., Chabaux F., Van der Woerd J., Viville D., Pelt E., Kali E., Lerouge C., Ackerer P., di Chiara Roupert R., Négrel P. (2016) Regolith evolution on the millennial timescale from combined U–Th–Ra isotopes and in situ cosmogenic 10Be analysis in a weathering profile (Strengbach catchment, France). Earth Planet. Sci. Lett. 453, 33–43.

Andersen M.B., Erel Y., Bourdon B. (2009) Experimental evidence for 234U–238U fractionation during granite weathering with implications for $^{234}U/^{238}U$ in natural waters. Geochim. Cosmochim. Acta 73, 4124–4141.

Berner R.A. (1997) The rise of plants and their effect on weathering and atmospheric CO2. Science 276, 544-546.

Bosia C. (2016) Les séries radioactives de l'uranium dans les sédiments de la rivière Gandak (Himalaya): de la roche totale aux analyses in situ sur les minéraux séparés. Ph. D. thesis, Strasbourg Univ.

Bosia C., Chabaux F., Pelt E., Cogez A., Stille P., Deloule E., France-Lanord C. (2018) U-series disequilibria in minerals from Gandak River sediments (Himalaya). Chem. Geol. 477, 22–34.

Bourdon B., Bureau S., Andersen M. B., Pili E. and Hubert A. (2009) Weathering rates from top to bottom in a carbonate environment. Chem. Geol. 258, 275–287.

Brantley S.L., Chesley J.T., Stillings L.L. (1998) Isotopic ratios and release rates of strontium measured from weathering feldspars. Geochim. Cosmochim. Acta 62, 1493–1500.

Bullen T., White A., Blum A., Harden J., Schulz M. (1997) Chemical weathering of a soil chronosequence on granitoid alluvium: II. Mineralogic and isotopic constraints on the behavior of strontium. Geochim. Cosmochim. Acta61, 291–306.

Buss H.L., Chapela Lara M. Moore O.W., Kurtz A.C., Schulzb M.S., White A.F. (2017) Lithological influences on contemporary and long-term regolith weathering at the Luquillo Critical Zone Observatory. Geochim. Cosmochim. Acta 196,, 224–251.

Buss H.L., Sak P.B., Webb S.M., Brantley S.L. (2008) Weathering of the Rio Blanco quartz diorite, Luquillo Mountains, Puerto Rico: coupling oxidation, dissolution, and fracturing. Geochim. Cosmochim. Acta 72, 4488–4507.

Calvaruso, C., Mareschal, L., Turpault, M.-P., Leclerc, E., (2009). Rapid Clay Weathering in the Rhizosphere of Norway Spruce and Oak in an Acid Forest Ecosystem. Soil Sci. Soc. Am. J. 73, 331-338.

Carpentier M., Gannoun A., Pin C., Sigmarsson O., (2016). New thorium isotope ratio measurements in silicate reference materials: A-THO, AGV-2, BCR-2, BE-N, BHVO-2 and BIR-1. Geostand. Geoanal. Res. 40, 239–256

703 Chabaux F., Ben Othman D., J.L. Birck (1994) A new Ra-Ba chromatographic separation and
704 its application for the Ra mass spectrometric maesurement in recent volcanic rocks.
705 Chem. Geol. 114, 191-197. Erratum (1994) Chem. Geol. 116, 301.
706 Chabaux F., Blaes E., Stille P., di Chiara Roupert R., Pelt E., Dosseto A., Ma L., Buss H.L. and
707 Brantley S.L. (2013) Regolith formation rate from U-series nuclides: Implications from
708 the study of a spheroidal weathering profile in the Rio Icacos watershed (Puerto Rico).
709 Geochim. Cosmochim. Acta 100, 73-95.
710 Chabaux F., Bourdon B. and Riotte J. (2008) U-Series Geochemistry in Weathering Profiles,
711 River Waters and Lakes. In: *Radioactivity in the Environment* (Eds. S. Krishnaswami and
712 J.K. Cochran). Elsevier, 49-104.
713 Chabaux F., Dequincey O., Lévèque J.-J., Leprun J.-C., Clauer N., Riotte J. and Paquet H.
714 (2003b) Tracing and dating recent chemical transfers in weathering profiles by trace-
715 element geochemistry and ^{238}U-^{234}U-^{230}Th disequilibria: the example of the Kaya lateritic
716 toposequence (Burkina-Faso). C. R. Geosci. 335, 1219-1231.
717 Chabaux F., Riotte J. and Dequincey O. (2003a) Fractionation during weathering and river
718 transport. *Reviews in Mineralogy and Geochemistry* 52, 533-576.
719 Cheng, H., Edwards, R.L., Hoff, J., Gallup, C.D., Richards, D.A., Asmerom, Y. (2000). The half-
720 lives of uranium-234 and thorium-230. Chem. Geol. 169, 17–33.
721 Clow D.W., Drever J.I. (1996) Weathering rates as a function of flow through an alpine soil.
722 Chem. Geol. 132, 131 – 141.
723 Cogez A., Herman F., Pelt E., Reuschlé T., Morvan G., Darvill C.M., Norton K.P., Christl M.,
724 Märki L., Chabaux F. (2018) U–Th and 10 Be constraints on sediment recycling in
725 proglacial settings, Lago Buenos Aires, Patagonia. Earth Surf. Dynam., 6, 121–
726 140.Condomines, M., Tanguy, J.C., Michaud, V., (1995). Magma dynamics at Mt Etna:
727 Constraints from U–Th–Ra–Pb radioactive disequilibria and Sr isotopes in historical
728 lavas. Earth and Planet. Sci. Let. 132, 25–41.
729 Cornelis, J.T., Ranger, J., Iserentant, A., Delvaux, B., (2010). Tree species impact the
730 terrestrial cycle of silicon through various uptakes. Biogeochemistry. 97, 231-245.
731 Cornu S., Lucas Y., Lebon E., Ambrosi J. P., Luizao F., Rouiller J., Bonnay M. and Neal C. (1999)
732 Evidence of titanium mobility in soil profiles, Manaus, central Amazonia. Geoderma 91,
733 281–295Dahl P.S. (1996) The crystal-chemical basis for Ar retention in micas: inferences
734 from interlayer partitioning and implications for geochronology. Contrib Mineral Petrol
735 123, 22–39.
736 Delanghe, D., Bard, E., Hamelin, B. (2002). New TIMS constraints on the uranium-238 and
737 uranium-234 in seawaters from the main ocean basins and the Mediterranean Sea.
738 Marine Chem. 80, 79–93.
739 DePaolo D.J., Maher K., Christensen J.N. and McManus J. (2006) Sediment transport time
740 measured with U-series isotopes: Results from ODP North Atlantic drift site 984. Earth
741 Planet. Sci. Lett. 248, 394-410.

742 Dequincey, O., Chabaux, F., Clauer, N., Sigmarsson, O., Liewig, N., Leprun, J.C., (2002).
743 Chemical mobilizations in laterites: evidence from trace elements and ^{238}U-^{234}U-^{230}Th
744 disequilibria. Geochim. Cosmochim. Acta. 66, 1197-1210.
745 Dosseto A., Buss H. L. and Chabaux F. (2014) Age and weathering rate of sediments in small
746 catchments: the role of hillslope erosion. Geochim. Cosmochim. Acta 132, 238–258.
747 Dosseto A., Turner S.P., Chappell J. (2008) The evolution of weathering profiles through time:
748 New insights from uranium-series isotopes. Earth Planet. Sci. Lett. 274, 359-371.
749 Dosseto, A, Menozzi D., Kinsley L.P.J. (2019) Age and rate of weathering determined using
750 uranium-series isotopes: Testing various approaches. Geochim. Cosmochim. Acta 246,
751 213-233.
752 Dosseto, A., Buss, H.L., Suresh, P.O. (2012) Rapid regolith formation over volcanic bedrock
753 and implications for landscape evolution. Earth Planet. Sci. Lett. 337–338, 47-55.
754 Drever J.I. and Hurcomb D.R. (1986) Neutralization of atmospheric acidity by chemical
755 weathering in an alpine drainage basin in the North Cascade Mountains. Geology 14,
756 221-224.
757 Fichter, J., Bonnaud P., Turpault M.P. and Ranger J. (1998) Quantitative determination of
758 minerals in acid forest soils of granite. J. Plant Nutr. Soil Sci. 161, 129-39.
759 Gaillardet, J., Dupré, B., Louvat, P., and Allègre,C. J. (1999) Global silicate weathering and
760 CO2 consumption rates deduced from the chemistry of large rivers. Chemical Geology
761 159, 3-30.
762 Ghaleb, B., Pons-Branchu, E.,Deschamps, P. (2004).Improved method for radium extraction
763 from environmental samples and its analysis by thermal ionization mass spectrometry. J.
764 Anal. At. Spectrom. 7, 906–910.
765 Gontier, A., Rihs, S., Chabaux, F., Lemarchand, D., Pelt, E., Turpault, M-P. (2015). Lack of
766 bedrock grain size influence on the soil production rate. Geochim. Cosmo. Acta. 166,
767 146-164.
768 Govindaraju, K. (1994). Compilation of working values and sample description for 383
769 geostandards. Geostandards Newsletter 18, 1–158.
770 Granet, M., Chabaux, F., Stille, P., France-Lanord, C., Pelt, E. (2007). Time-scales of
771 sedimentary transfer and weathering processes from U-series nuclides: Clues from the
772 Himalayan rivers. Earth Planet. Sci. Lett. 261, 389-406.
773 Haward S.J., Smits M.M., Vala Ragnarsdottir K., Leake J.R., Banwart S.A. McMaster T.J.
774 (2011), In situ atomic force microscopy measurements of biotite basal plane reactivity in
775 the presence of oxalic acid. Geochim. Cosmochim. Acta 75, 6870–6881.
776 Hellmann, R., Wirth, R., Daval, D., Barnes, J.-P., Penisson, J.-M., Tisserand, D., Epicier, T.,
777 Florin, B., Hervig, R.L. (2012) Unifying natural and laboratory chemical weathering with
778 interfacial dissolution–reprecipitation: a study based on the nanometer-scale chemistry
779 of fluid–silicate interfaces. Chem. Geol. 294–295, 203–216
780 Hinsinger P., Jaillard B. and Dufey J.E. (1992) Rapid Weathering of a Trioctahedral Mica by
781 the Roots of Ryegrass. Soil Sci. Soc. Am. J. 56, 977-982.

Hochella Jr., M.F., Banfield, J.F., (1995). Chemical weathering of silicates in nature: a microscopic perspective with theoretical considerations. In: Ribbe, P.H. (Ed.), Chemical Weathering Rates of Silicate Minerals. Reviews in Mineralogy. Mineralogical Society of America, Washington, D.C., pp. 353–406.

Holden N.E. (1990) Total half-lives for selected nuclides. Pure Appl. Chem. 6, 941–958.

Jaffey A.H., Flynn K.F., Glendenin L.E., Bentley W.C., Essling A.M. (1971) Precision measurement of half-lives and specific activities of ^{235}U and ^{238}U. Phys. Rev. C 4, 1889–1906.

Jaffrain J. (2006) Effet des essences forestières sur le fonctionnement organo-minéral d'un sol acide: observations et modélisation. Ph. D. Thesis, Nancy I Univ.

Jeanbrun, M., Pourcelot, L., Mercat, C., Boulet, B., Pelt, E., Chabaux, F., Cagnat, X., Gauthier-Lafaye, F. (2012). Potential sources affecting the activity concentrations of ^{238}U, ^{235}U, ^{232}Th and some decay products in lettuce and wheat samples. J. Environ. Monit. 14, 2902-2912.

Keech, A.R., West, A.J., Pett-Ridge, J.C., and Henderson, G.M., (2013) Evaluating U-series tools for weathering rate and duration on a soil sequence of known ages. Earth Planet. Sci. Lett. 374, 24-35.

Kigoshi K. (1971) Alpha recoil thorium-234: dissolution into water and uranium-234/uranium-238 disequilibrium in nature. Science 173, 47–49

Koornneef J.M., Stracke A., Aciego S., Reubi O., Bourdon B. (2010) A new method for U–Th–Pa–Ra separation and accurate measurement of ^{234}U–^{230}Th–^{231}Pa–^{226}Ra disequilibria in volcanic rocks by MC-ICPMS. Chem. Geol. 277, 30–41.

Lemarchand, D., Cividini, D., Turpault, M.P., Chabaux F. (2012) Boron isotopes in different grain size fractions: Exploring past and present water–rock interactions from two soil profiles (Strengbach, Vosges Mountains) Geochim. Cosmo. Acta 98, 78-93.

Leyval C. and Berthelin J. (1991) Weathering of a Mica by Roots and Rhizospheric Microorganisms of Pine. Soil Sci. Soc. Am. J. 55, 1009-1016.

Ma, L., Chabaux, F., Pelt, E., Blaes, E., Jin, L., Brantley, S. (2010) Regolith production rates calculated with uranium-series isotopes at Susquehanna/Shale Hills Critical Zone Observatory. Earth Planet. Sci. Lett. 297, 211-225.

Ma, L., Chabaux, F., Pelt, E., Granet, M., Sak, P.B., Gaillardet, J., Lebedeva, M., Brantley, S.L., (2012). The effect of curvature on weathering rind formation: Evidence from Uranium-series isotopes in basaltic andesite weathering clasts in Guadeloupe. Geochim. Cosmochim. Acta 80, 92-107.

Ma, L., Chabaux, F., West, N., Kirby, E., Jin, L., Brantley, S. (2013) Regolith production and transport in the Susquehanna Shale Hills Critical Zone Observatory, Part 1: Insights from U-series isotopes. Journal of Geophysical Research, Earth Surface. 118, 722-740.

Maher K., DePaolo D.J., Christensen J.N. (2006b) U–Sr isotopic speedometer: Fluid flow and chemical weathering rates in aquifers. Geochim. Cosmochim. Acta 70, 4417–4435.

821 Maher K., DePaolo D.J., Lin C-F. (2004) Rates of silicate dissolution in deep-sea sediment: in
822 situ measurement using 234U/238 U of pore fluids. Geochim Cosmochim Acta 68, 4629–
823 4648.
824 Maher K., Steefel C., White A.F., Stonestrom D.A. (2009) The role of reaction affinity and
825 secondary minerals in regulating chemical weathering rates at the Santa Cruz Soil
826 Chronosequence, California. Geochim. Cosmochim. Acta 73, 2804–2831.
827 Maher K., Steefel C.I., DePaolo D.J., Viani B.E. (2006a) The mineral dissolution rate
828 conundrum: insights from reactive transport modeling of U isotopes and pore fluid
829 chemistry in marine sediments. Geochim Cosmochim Acta 70, 337–363.
830 Mareschal, L., (2008). Effet des substitutions d'essences forestières sur l'évolution des sols et
831 de leur minéralogie: bilan après 28 ans dans le site expérimental de Breuil (Morvan). Ph.
832 D Thesis, Nancy I Univ.
833 Mareschal, L., Bonnaud, P., Turpault, M.P., Ranger, J., (2010). Impact of common European
834 tree species on the chemical and physicochemical properties of fine earth: an unusual
835 pattern. Eur. J. Soil Sci. 61, 14-23.
836 Mareschal, L., Ranger, J., Turpault, M.-P. (2015). Effect of granite crystal grain size on soil
837 properties and pedogenic processes. Geoderma 249-250, 12-20.
838 Martin D., Lal T., Sachdev C.B. and Sharma J.P. (2010) Soil organic carbon storage changes
839 with climate change, landform and land use conditions in Garhwal hills of the Indian
840 Himalayan mountains. Agriculture, Ecosystems & Environment 138, 64-73.
841 Menozzi D. (2016) Assessment of Sequential Extraction and Mineral Separation for studying
842 Uranium-Series Isotopes in Regolith. Ph D thesis. Univ Wollongong, Australia.
843 Meunier A. (2005) Clays. Springer Berlin.
844 Millot R., Vigier N., Gaillardet J. (2010) Behaviour of lithium and its isotopes during
845 weathering in the Mackenzie Basin, Canada. Geochim. Cosmo. Acta 74 3897-3912
846 Murphy S.F., Brantley S.L., Blum A.E., White A.F., Dong H. (1998) Chemical weathering in a
847 tropical watershed, Luquillo Mountains, Puerto Rico: II. Rate and mechanism of bioitite
848 weathering. Geochim. Cosmochim. Acta 62, 227 – 243
849 Newman ACD (1969) Cation exchange properties of micas. I. The relation between mica
850 composition and potassium exchange in solutions of different pH. J.Soil. Sci. 20, 357-
851 373.
852 Newman ACD, Brown G (1966) Chemical changes during the alteration of micas. Clay Miner.
853 23:337–342
854 Olander D.R., Eyal Y. (1990a) Leaching of uranium and thorium from monazite: II. Elemental
855 leaching. Geochim. Cosmochim. Acta 54, 1879-1887.
856 Paces, T. (1983). Rate Constants of Dissolution Derived from the Measurements of Mass
857 Balance in Hydrological Catchments. Geochim Cosmochim Ac 47, 1855-1863.
858 Pelt, E., Chabaux, F., Innocent, C., Navarre-Sitchler, A.K., Sak, P.B., Brantley, S.L., (2008).
859 Uranium-thorium chronometry of weathering rinds: Rock alteration rate and paleo-
860 isotopic record of weathering fluids. Earth Planet. Sci. Lett. 276, 98-105.

Pelt, E., Chabaux, F., Stille, P., Innocent, C., Ghaleb, B., Girard, M., Guntzer, F., (2013). Atmospheric dust contribution to the budget of U-series nuclides in soils from the Mount Cameroon volcano. Chem. Geol. 341, 147-157.

Rezzoug, S., Fernex, F., Michel, H., Barci-Funel, G., Barci, V., (2009). Behavior of uranium and thorium isotopes in soils of the Boréon area, Mercantour Massif (S.E. France): Leaching and weathering rate modeling. J. Radioanal. Nucl. Chem. 279, 801-809.

Rihs S., Gontier A., Pelt E., Fries D., Turpault M-P. Chabaux F. (2016a) Behavior of U and Th series nuclides in soils during a land cover change. Chem. Geol. *441,* 106-123.

Rihs, S., Prunier, J., Thien, B., Lemarchand, D., Pierret, M.-C., Chabaux, F., (2011). Using short-lived nuclides of the U- and Th-series to probe the kinetics of colloid migration in forested soils. Geochim. Cosmochim. Acta. 75, 7707-7724.

Rubin, K.H. (2001). Analysis of 232Th/230Th in volcanic rocks: a comparison of thermal ionization mass spectrometry and other methodologies. Chem. Geol. 175, 723–750.

Schön R., Winkler G., Kutschera W. (2004). A critical review of experimental data for the half-lives of the uranium isotopes 238U and 235U. Appl. Radiat. Isot. 60, 263–273.Schwertmann, U., (1964). Differenzierung der Eisenoxide des Bodens durch Extraktion mit Ammoniumoxalat-Lösung. Zeitschrift für Pflanzenernährung, Düngung, Bodenkunde. 105, 194-202.

Seddoh, F.K. (1973). Altération des roches cristallines du Morvan (granite, granophyres, rhyolites). Etude minéralogique, géochimique et micro-morphologique. Ph. D. Thesis, Dijon Univ.

Sims, K.W.W., Gill, J.B., Dosseto, A., Hoffmann, D.L., Lundstrom, C.C., Williams, R.W., Ball, L., Tollstrup, D., Turner, S., Prytulak, J., Glessner, J.J.G., Standish, J.J., Elliott, T., (2008). An Inter-Laboratory Assessment of the Thorium Isotopic Composition of Synthetic and Rock Reference Materials. Geostand. Geoanal. Res. 32, 65-91.

Suresh P., Dosseto A., Hesse P., Handley H. (2013) Soil formation rates determined from Uranium-series isotope disequilibria in soil profiles from the southeastern Australian highlands. Earth Planet. Sci. Lett. 379, 26-37.

Tamm O. (1922) Um best ämning ow de oorganiska komponenterna i markens gelcomplex. Medd. Statens Skogsförsökanst. 19, 385-404.

Taboada T., Cortizas A. M., Garcıa C. and Garcıa-Rodeja E. (2006) Particle-size fractionation of titanium and zirconium during weathering and pedogenesis of granitic rocks in NW Spain. Geoderma131, 218–236.

Taylor A., Blum J., Lasaga A. (2000a) The dependence of labradorite dissolution and Sr isotope release rates on solution saturation state Geochim. Cosmochim. Acta 64, 2389 – 2400.

Taylor A., Blum J., Lasaga A., MacInnis I. (2000b) Kinetics of dissolution and Sr release during biotite and phlogopite weathering. Geochim. Cosmochim. Acta 64, 1191–1208.

Taylor, A., Blum, J.D., (1995). Relation between Soil Age and Silicate Weathering Rates Determined from the Chemical Evolution of a Glacial Chronosequence. Geology 23, 979-982.

902 Turpault M.P, Fichter J., Ezzaïm A., Ranger J. (1998) Quantitative mineralogy of acidic soils.
903 Congrès mondial de science du sol, 20-26/08, Montpellier, France
904 Turpault M.P. and Trotignon L. (1994) The dissolution of biotite single crystals in dilute HNO_3
905 at 24°C: evidence of an anisotropic corrosion process of micas in acidic solutions.
906 Geochim Cosmochim Acta 58, 2761-2775.
907 Vigier N., Bourdon B., Turner S. P. and Allegre C. J. (2001) Erosion timescales derived from U-
908 decay series measurements in rivers. Earth Planet. Sci. Lett. 193, 549-563.
909 Vigier, N., Bourdon, B., (2011). Constraining Rates of Chemical and Physical Erosion Using U-
910 Series Radionuclides. In: Baskaran, M. (Ed.), Handbook of Environmental Isotope
911 Geochemistry. Advances in Isotope Geochemistry. Springer Berlin Heidelberg, pp. 553-
912 571.
913 Voinot A. (2012) Contribution des isotopes du bore à l'étude des mécanismes et bilans de
914 l'altération des minéraux des sols Ph. D. Thesis, Strasbourg Univ.
915 Wan J., Tokunaga T. K., Ashby P. D., Kim Y., Voltolini M., Gilbert B. and DePaolo D. J. (2018)
916 Supercritical CO2 uptake by nonswelling phyllosilicates. Proc. Natl. Acad. Sci. U. S. A.,
917 115, 873–878
918 White A. F. and Buss H. L. (2014) Natural weathering rates of silicate minerals. InTreatise on
919 Geochemistry (Second Edition) (ed. J. I. Drever) vol 7. Elsevier, Oxford, pp. 115–155
920 White A.F. (2002) Determining mineral weathering rates based on solid and solute
921 weathering gradients and velocities: application to biotite weathering in saprolites.
922 Chem. Geol. 190, 69 – 89.
923 White A.F. and Brantley S.L. (2003) The effect of time on the weathering of silicate minerals:
924 why do weathering rates differ in the laboratory and field? Chem. Geol. 202, 479-506
925 White A.F., Blum A.E., Schulz M.S., Vivit D.V., Stonestrom D.A., Larsen M., Murphy S.F., Eberl
926 D. (1998) Chemical weathering in a tropical watershed, Luquillo Mountains, Puerto
927 Rico: I. Long-term versus short-term weathering fluxes. Geochim. Cosmochim. Acta 62,
928 209-226.
929 White A.F., Schulz M.S., Lawrence C.R., Vivit D.V., Stonestrom D.A. (2017). Long-term
930 flowthrough column experiments and their relevance to natural granitoid weathering
931 rates. Geochim Cosmochim Acta 202, 190-214.
932 Williams, R.W., Collerson, K.D., Gill, J.B., Deniel, C. (1992). High Th/U ratios in subcontinental
933 lithospheric mantle: mass spectrometric measurement of Th isotopes in Gaussberg
934 lamproites. Earth and Planet. Sci. Lett. 111, 257–268.
935

Figure captions

Fig. 1: Location of the experimental Breuil-Chenue INRA site and of soil profiles developed under the native forest from which biotite grains were extracted. The profiles studied by Rihs, Gontier et al. (2016) under the substituted Oak stand are also reported (short-term weathering rate, see the text for explanation).

Fig. 2: Mass fraction of the remaining parent biotite and weathering products in the study grains without quartz contributions (from Voinot 2012).

Figure 3: Evolution of Th and U contents in the grains relative to the K_2O contents.

Figure 4: Evolution of U/Th ratios in the grains relative to the fraction of remaining parent biotite (a) or TiO_2 contents (b).

Figure 5: Evolution of ($^{234}U/^{238}U$) ratios in the grains relative to the fraction of remaining parent biotite present (quartz excepted, see the text for explanation). ($^{234}U/^{238}U$) ratios in the 20-30 cm (> 200 µm) and the saprolite samples are inconsistent with the weathering stage deduced from major elements.

Figure 6: U-series disequilibria measured and modeled from the separated grains. Model 1 and model 2 stand for the two extreme models derived from the range of solutions allowing for a description of the data. Lengths of time required for evolution from the 120-140 cm to the 20-30 cm (50-200 µm) samples are modeled as 6 and 52 ky in models 1 and 2, respectively.

Figure 7: Measured and modeled U (a) and Th (b) isotopic ratios vs ($^{238}U/^{232}Th$) ratios in the separated grains. "Model het. U/Th" accounts for a potential initial U/Th heterogeneity and corresponds to a model with a slightly different initial ($^{238}U/^{232}Th$) ratio (0.37 instead of 0.48, see the text for explanation). The equiline denotes the radioactive equilibrium.

Figure 8: Sets of Eq. 2 solutions allowing for the reproduction of measured activity ratios. For each set of solutions, ratios between the ^{238}U, ^{234}U and ^{230}Th leaching constants are reported as a function of the length of time required for evolution from least to most weathered sample.

Figure 9: Comparison of measured biotite weathering rates with previously reported experimental and field rates (adapted from White and Brantley, 2003 and references therein; Föllmi et al., 2009; Buss et al., 2008, Dosseto et al., 2014, 2019). The dashed-line represents the power function proposed by White and Brantley (2003). The "land cover change" data corresponds to the biotite weathering rate induced by an experimental substitution of vegetation 35 years ago within the same site as that studied here (Rihs, Gontier et al., 2016). The "field Swiss Alp" data report rates from sedimentary chronosequences of the Rhône and Oberaar Glaciers (Föllmi et al., 2009). The "U-series derived rates" ranges report data derived from U-series weathering rates determinations (Dosseto et al., 2014, 2019).

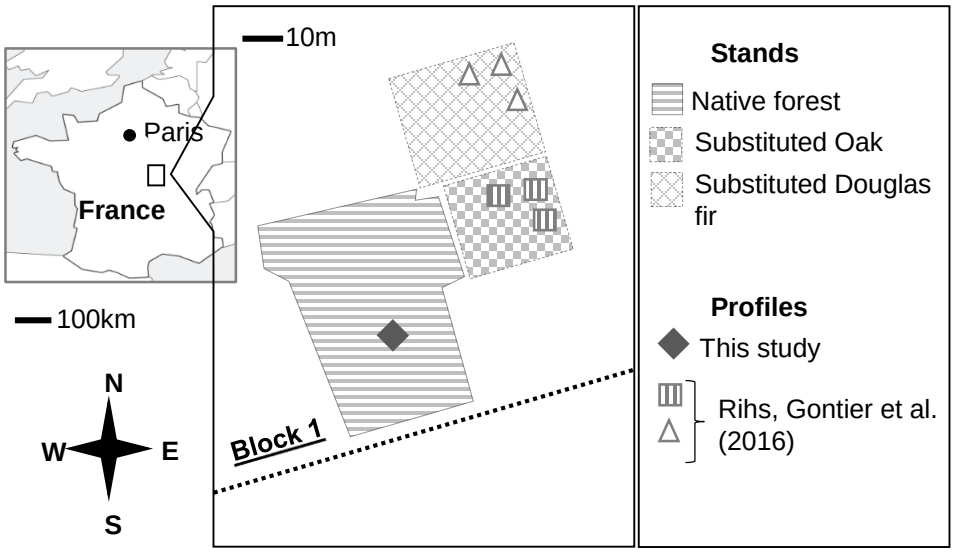


Fig. 1: Location of the experimental Breuil-Chenue INRA site and of soil profiles developed under the native forest from which biotite grains were extracted. The profiles studied by Rihs, Gontier et al. (2016) under the substituted Oak stand are also reported (short-term weathering rate, see the text for explanation).

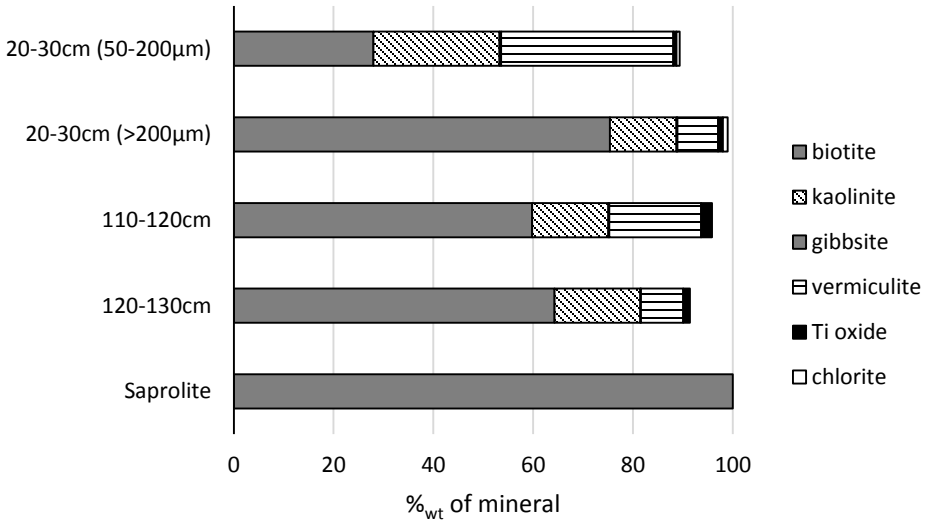


Fig. 2: Mass fraction of the remaining parent biotite and weathering products in the study grains without quartz contributions (from Voinot 2012).

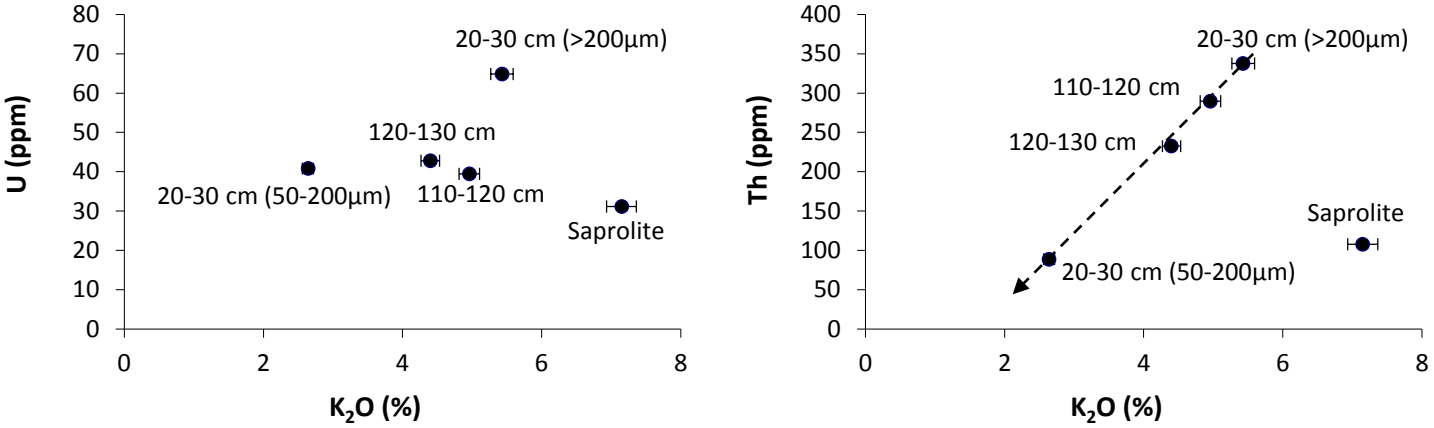


Figure 3 : Evolution of Th and U contents in the grains relative to the K_2O contents.

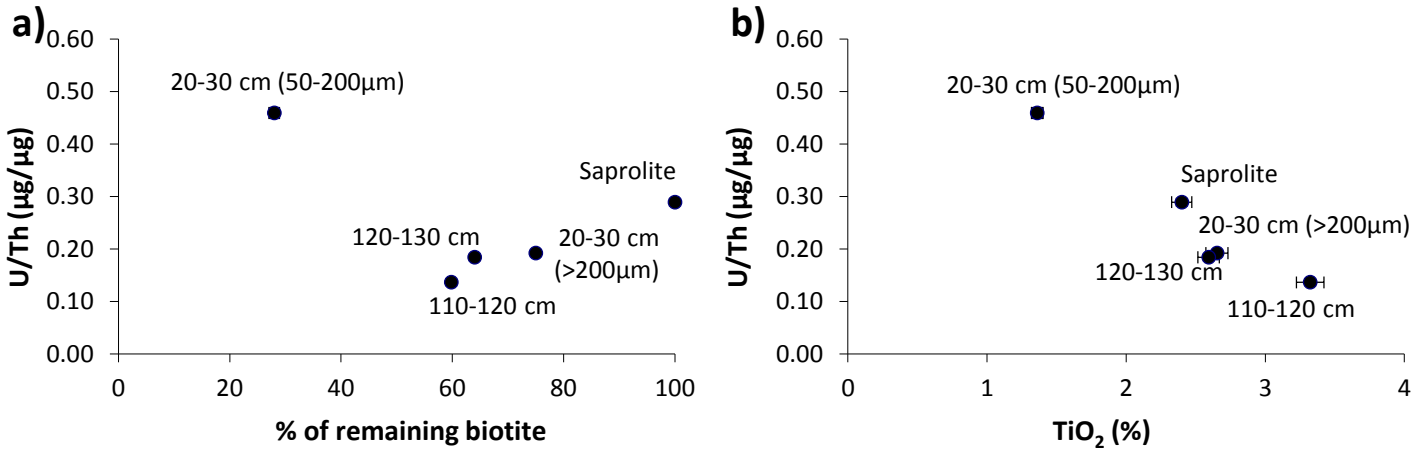


Figure 4: Evolution of U/Th ratios in the grains relative to the fraction of remaining parent biotite (a) or TiO_2 contents (b).

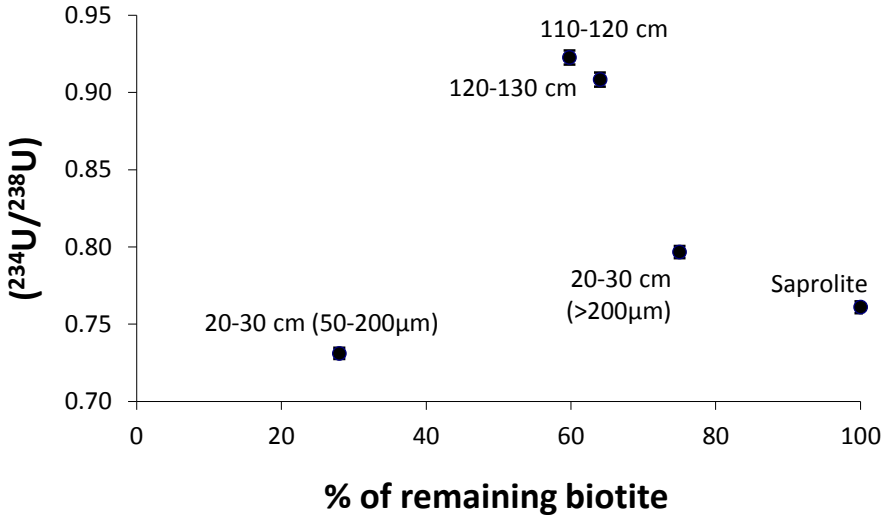
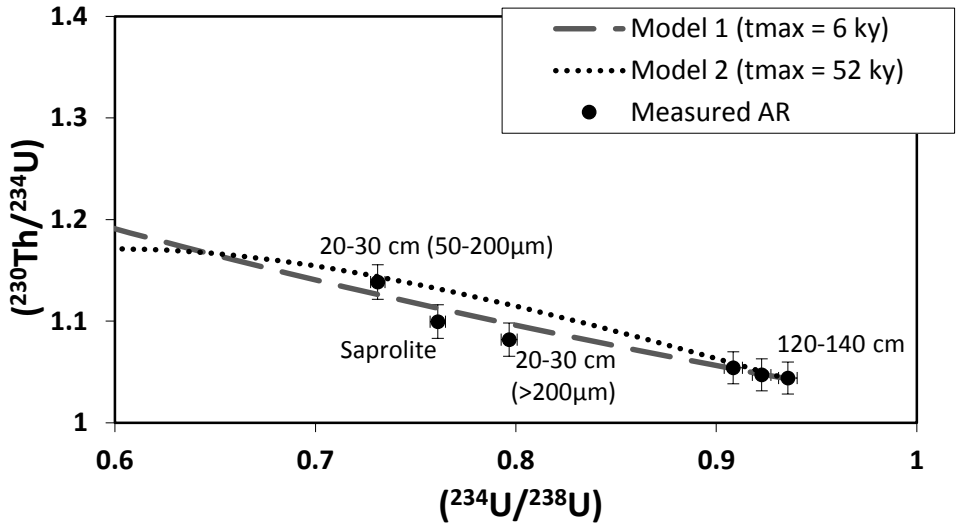


Figure 5: Evolution of ($^{234}U/^{238}U$) ratios in the grains relative to the fraction of remaining parent biotite present (quartz excepted, see the text for explanation). ($^{234}U/^{238}U$) ratios in the 20-30 cm (> 200 µm) and the saprolite samples are inconsistent with the weathering stage deduced from major elements.



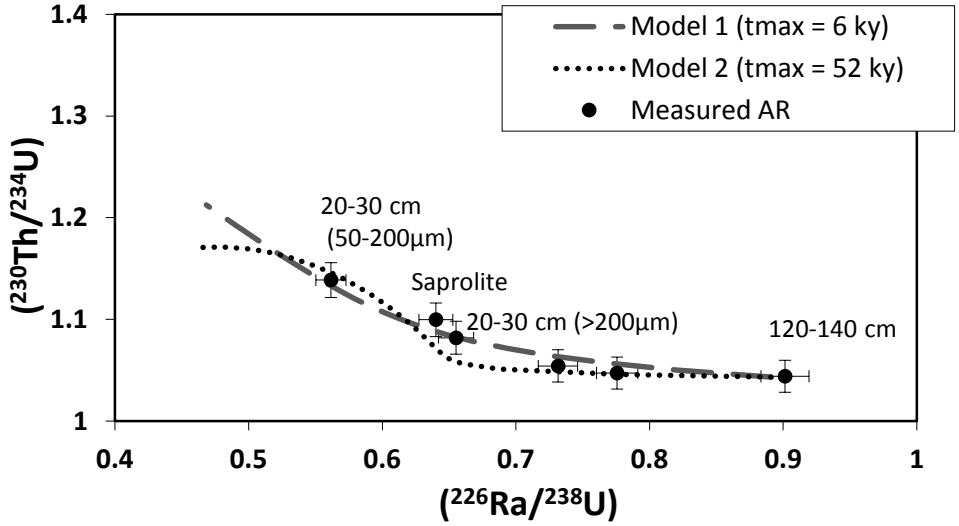


Figure 6: U-series disequilibria measured and modeled from the separated grains. Model 1 and model 2 stand for the two extreme models derived from the range of solutions allowing for a description of the data. Lengths of time required for evolution from the 120-140 cm to the 20-30 cm (50-200 µm) samples are modeled as 6 and 52 ky in models 1 and 2, respectively.

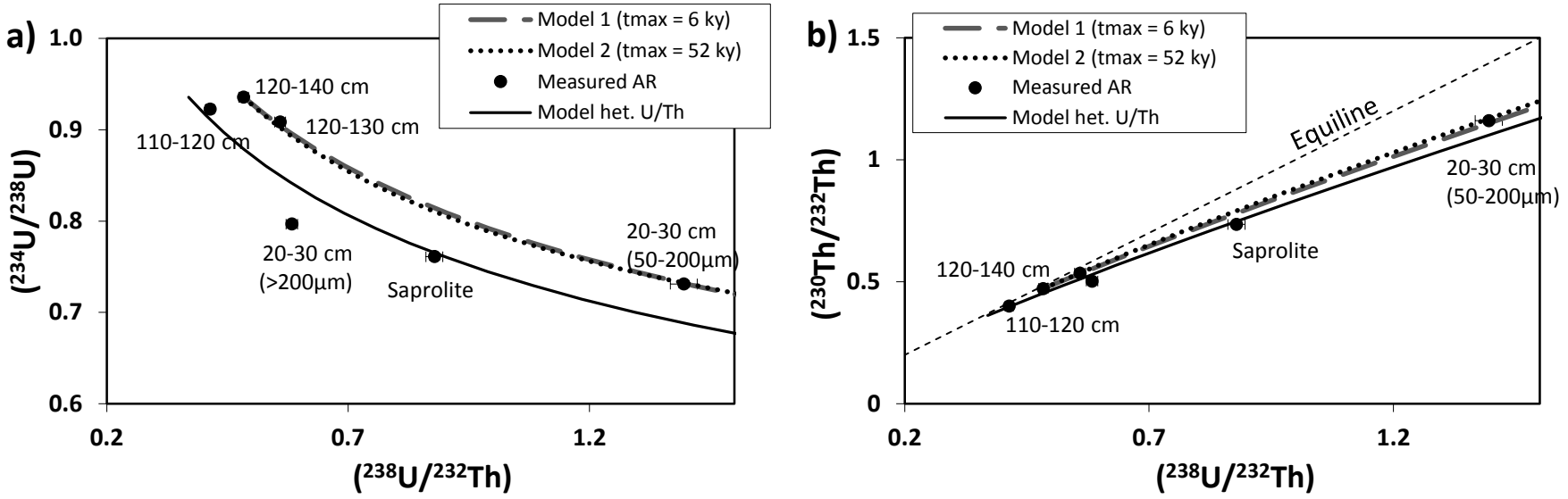


Figure 7: Measured and modeled U (a) and Th (b) isotopic ratios vs ($^{238}U/^{232}Th$) ratios in the separated grains. "Model het. U/Th" accounts for a potential initial U/Th heterogeneity and corresponds to a model with a slightly different initial ($^{238}U/^{232}Th$) ratio (0.37 instead of 0.48, see the text for explanation). The equiline denotes the radioactive equilibrium.

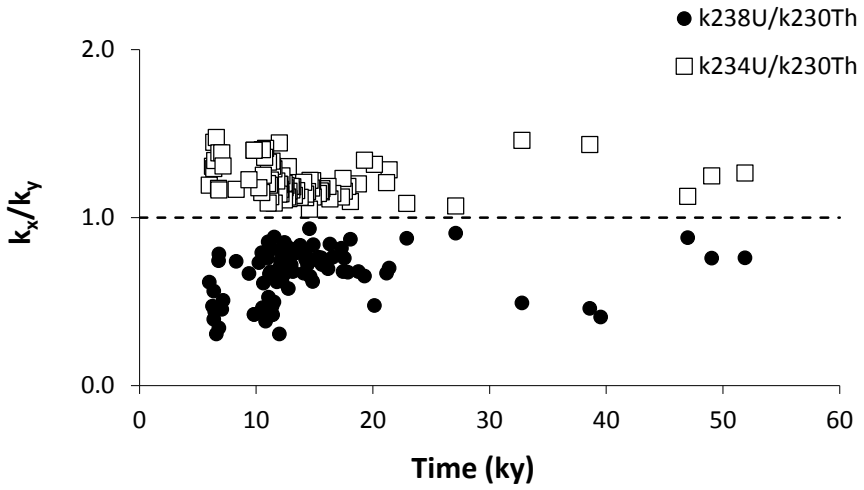


Figure 8: Sets of Eq. 2 solutions allowing for the reproduction of measured activity ratios. For each set of solutions, ratios between the ^{238}U, ^{234}U and ^{230}Th leaching constants are reported as a function of the length of time required for evolution from least to most weathered sample.

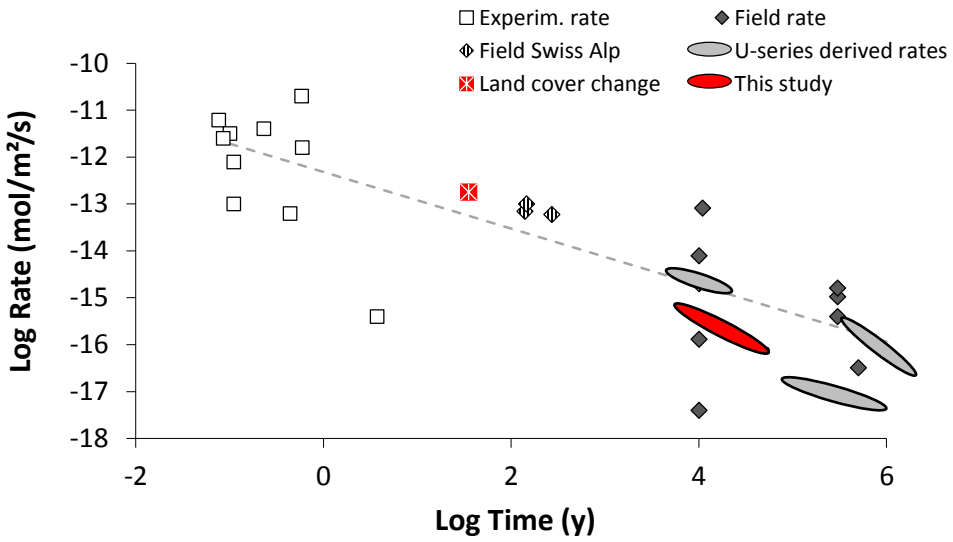


Figure 9: Comparison of measured biotite weathering rates with previously reported experimental and field rates (adapted from White and Brantley, 2003 and references therein; Föllmi et al., 2009; Buss et al., 2008, Dosseto et al., 2014, 2019). The dashed-line represents the power function proposed by White and Brantley (2003). The "land cover change" data corresponds to the biotite weathering rate induced by an experimental substitution of vegetation 35 years ago within the same site as that studied here (Rihs, Gontier et al., 2016). The "field Swiss Alp" data report rates from sedimentary chronosequences of the Rhône and Oberaar Glaciers (Föllmi et al., 2009). The "U-series derived rates" ranges report data derived from U-series weathering rates determinations (Dosseto et al., 2014, 2019).

Table 1: U- and Th-series nuclides concentrations and activity ratios measured in the standard rocks between 2012 and 2014.

Standard/date	[U] µg.g^{-1}	[Th] µg.g^{-}	[^{226}Ra] fg.g^{-1}	(^{234}U/^{238}U)	2SE	(^{230}Th/^{232}Th)	2SE	(^{230}Th/^{234}U)	(^{226}Ra/^{230}Th)	(^{238}U/^{232}Th)
BE-N										
01/2012 [b]	2.498 [c]	10.55 [d]	835 [c]	0.996	0.002	0.728	0.003	1.015	0.980	0.721
04/2012 [b]	2.499 [c]	10.59 [d]	nd	0.997	0.003	0.727	0.003	1.015	nd	0.718
10/2012 [b]	2.507 [c]	10.49 [d]	844 [c]	0.998	0.003	0.728	0.004	1.003	0.997	0.727
Mean	2.502	10.54	840	0.997		0.728		1.011	0.988	0.722
2 RSD (%)	0.4	1.0	1.5	0.2		0.2		1.4	2.4	1.3
BCR-2										
05/2013	1.713 [d]	5.902 [d]	573 [c]	1.0009	0.0006	0.883	0.004	0.999	0.992	0.883
05/2013	1.711 [d]	5.890 [d]	574 [c]	1.0001	0.0006	0.885	0.003	1.001	0.993	0.884
12/2013 [a]	1.700 [d]	5.897 [d]	574 [c]	1.0001	0.0006	0.886	0.004	1.010	0.991	0.877
03/2014	1.699 [d]	5.901 [d]	572 [c]	0.9988	0.0007	0.880 [e]	0.003	1.006 [e]	0.993 [e]	0.876
03/2014 [a]	1.690 [d]	5.876 [d]	572 [c]	1.0014	0.0019	0.881 [e]	0.003	1.005 [e]	0.996 [e]	0.875
06/2014	1.702 [d]	5.908 [d]	580 [c]	0.9957	0.0009	0.883 [e]	0.003	1.012 [e]	1.003 [e]	0.877
Mean	1.702	5.896	574	1.000		0.883		1.005	0.995	0.879
2 RSD (%)	1.0	0.4	1.1	0.4		0.5		1.0	0.9	0.9
2SD of relative deviations from the means (%)	0.8	0.6	1.1	0.3		0.4		1.0	1.2	0.9
Analytical uncertainties used in this study (%)	1.0	1.0	1.5	0.5		1.0		1.5	2.0	1.0

2SE are internal standard error from within-run counting statistics. The following radioactive decay constants were used: λ_{238}= 1.5513×10^{-10}y^{-1} (Jaffey et al., 1971; Schön et al., 2004), λ_{234}= 2.8263×10^{-6}y^{-1} (Cheng et al., 2000), λ_{230}= 9.158×10^{-6}y^{-1} (Cheng et al., 2000), λ_{226}= 4.335×10^{-4}y^{-1} (Holden, 1990) and λ_{232}= 4.932×10^{-11}y^{-1} (Rubin, 2001).

nd: not determined

[a] mean value published in Ackerer et al.(2016)

[b] mean value published in Claude et al.(2016)

[c] measured with a Thermo- Scientific Triton mass spectrometer (TIMS)

[d]measured with a Thermo- Scientific Neptune multiple collector inductively coupled plasma mass spectrometer (MC-ICP-MS)

[e] corrected from ^{232}Th peak tailing over ^{230}Th

Table 2: Major elements contents (in %) in the biotite grains extracted from various soil depths and from the granitic saprolite (after Voinot, 2012)

	LOI 1000°C	SiO_2 (SiO_2*)	Al_2O_3 (Al_2O_3*)	MgO (MgO*)	CaO (CaO*)	Fe_2O_3 (Fe_2O_3*)	MnO (MnO*)	TiO_2 (TiO_2*)	Na_2O (Na_2O*)	K_2O (K_2O*)	$\frac{SiO_2^*}{Al_2O_3^*}$	$\frac{K_2O^*}{Al_2O_3^*}$
20-30 cm (50-200µm)	11.15	34.8	21.7	5.68	0.07	22.7	0.73	1.36	0.18	2.64		
		(29.8)	(23.4)	(6.12)	(0.07)	(24.5)	(0.79)	(1.47)	(0.19)	(2.84)	1.27	0.12
20-30 cm (200-2000µm)	6.17	43.5	20.8	4.07	0.06	17.1	0.53	2.65	0.44	5.43		
		(34.5)	(24.1)	(4.72)	(0.07)	(19.8)	(0.61)	(3.08)	(0.51)	(6.30)	1.43	0.26
110-120 cm	6.41	41.1	19.9	5.45	< dl	18.7	0.47	3.32	0.26	4.96		
		(32.2)	(22.9)	(6.26)		(21.5)	(0.53)	(3.82)	(0.30)	(5.70)	1.41	0.25
120-130 cm	6.01	44.1	20.2	4.84	< dl	16.1	0.48	2.59	0.31	4.40		
		(32.2)	(24.5)	(5.87)		(19.5)	(0.59)	(3.15)	(0.37)	(5.34)	1.31	0.22
Saprolite biotite	2.94	43.0	18.9	4.22	0.10	19.0	0.50	2.40	0.70	7.15		
		(38.0)	(20.6)	(4.59)	(0.11)	(20.7)	(0.54)	(2.61)	(0.76)	(7.78)	1.86	0.38
Saprolite biotite after interlayer extraction (NaCl)[a]	10.33	40.0	15.1	3.40	1.15	15.4	0.44	1.75	6.2	4.05		

Results are given as percent fractions on weight basis after drying at 110°C per gram of extracted grains (quartz included, Voinot, 2012). The values in brackets (*) refer to the major element contents recalculated per gram of biotite and weathering products without quartz, i.e.; after subtracting quartz contribution to SiO_2 content. The precision is 3%.

LOI 1000°C: Lost on Ignition at 1000 °C.

dl = detection limit (= 0.05 %)

[a] this study

Table 3: U- and Th-series nuclides concentrations and activity ratios in the separated biotite grains.

	[U]	[Th]	($^{234}U/^{238}U$)	($^{230}Th/^{234}U$)	($^{226}Ra/^{230}Th$)	($^{230}Th/^{232}Th$)	Residual biotite [a]
	µg.g^{-1}	µg.g^{-1}					%
Uncertainties	± 1 %	± 1 %	± 0.5 %	± 1.5 %	± 2 %	± 1 %	
20-30 cm (50-200µm)	40.8	88.8	0.731	1.139	0.667	1.161	28
20-30 cm (200-2000µm)	64.9	337.6	0.797	1.082	0.752	0.503	75
110-120 cm	39.5	289.6	0.923	1.047	0.794	0.400	60
120-130 cm	42.8	232.6	0.908	1.054	0.756	0.535	64
120-140 cm	49.4	310.2	0.936	1.044	0.913	0.472	nd
Saprolite biotite	31.2	107.7	0.761	1.100	0.757	0.735	100
Saprolite biotite replicate	29.5	96.8	0.762	1.101	0.766	0.776	/

[a]: from Voinot (2012), recalculated without quartz contribution (see the text for explanation).

Table 4: U, Th and Mg (when relevant) recovery during interlayer (1 M NaCl) and amorphous Fe-Al-Mn oxy-hydroxides (0.2 M oxalate acid/ ammonium oxalate) extractions from the saprolite biotite.

	% U	% Th	% Mg
1st extraction interlayer	0.7	0.15	nd
2nd extraction interlayer	0.3	0.02	nd
3rd extraction interlayer	0.05	< dl	nd
Oxy-hydroxides extraction	2	4	0.4

The fractions are relative to the total amount of U, Th and Mg in the mineral. The 3 extractions with 1M NaCl lasted 7 days each and were sequential. The precision of the concentration measurement in the solutions is 10 % for U and Th (ICP-MS analysis) and 3 % for Mg (ICP-AES analysis).
nd: not determined
dl: detection limit

Table 5: Model parameter ranges allowing to fit the measured activity ratios. The leaching constants leading to the minimum and maximum time length are reported (model 1 and 2).

	$\mathbf{k}_{238U}$ (y^{-1})	$\mathbf{k}_{234U}$ (y^{-1})	$\mathbf{k}_{230Th}$ (y^{-1})	$\mathbf{k}_{226Ra}$ (y^{-1})	$\mathbf{k}_{232Th}$ (y^{-1})	Time[a]
Range	1.5×10^{-6} - 1.4×10^{-4}	7.6×10^{-6} - 1.5×10^{-4}	3.8×10^{-6} - 1.5×10^{-4}	1.7×10^{-4} - 3.7×10^{-4}	2×10^{-5} - 6×10^{-4}	6-52 ky
Model 1	4.50×10^{-5}	8.71×10^{-5}	7.29×10^{-5}	2.70×10^{-4}	2.24×10^{-4}	6 ky
Model 2	1.89×10^{-5}	2.42×10^{-5}	2.10×10^{-5}	2.30×10^{-4}	3.93×10^{-5}	52 ky

[a]: amount of time required to evolve from the 120-140 cm to the 20-30 cm (< 200 µm) sample